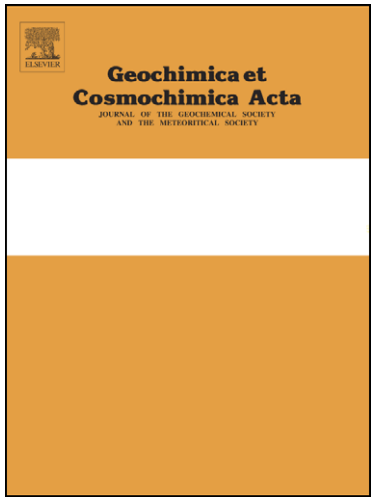

Calibration of cosmogenic ^{36}Cl production rates from Ca and K spallation in lava flows from Mt. Etna (38°N, Italy) and Payun Matru (36°S, Argentina)

Irene Schimmelpfennig, Lucilla Benedetti, Vincent Garreta, Raphaël Pik, Pierre-Henri Blard, Pete Burnard, Didier Bourlès, Robert Finkel, Katja Ammon, Tibor Dunai

PII: S0016-7037(11)00092-5
DOI: 10.1016/j.gca.2011.02.013
Reference: GCA 7092

To appear in: *Geochimica et Cosmochimica Acta*

Received Date: 21 January 2010
Accepted Date: 3 February 2011

Please cite this article as: Schimmelpfennig, I., Benedetti, L., Garreta, V., Pik, R., Blard, P-H., Burnard, P., Bourlès, D., Finkel, R., Ammon, K., Dunai, T., Calibration of cosmogenic ^{36}Cl production rates from Ca and K spallation in lava flows from Mt. Etna (38°N, Italy) and Payun Matru (36°S, Argentina), *Geochimica et Cosmochimica Acta* (2011), doi: 10.1016/j.gca.2011.02.013

Calibration of cosmogenic ^{36}Cl production rates from Ca and K spallation in lava flows from Mt. Etna (38°N, Italy) and Payun Matru (36°S, Argentina)

Irene Schimmelpfennig[a]*, Lucilla Benedetti[a], Vincent Garreta[a,c], Raphaël Pik[b], Pierre-Henri Blard[b], Pete Burnard[b], Didier Bourlès[a], Robert Finkel[a,e], Katja Ammon[d], Tibor Dunai[d]

[a] CEREGE, UMR 6635 CNRS, Université Paul Cézanne, Europôle de l'Arbois, 13545 Aix en Provence, France

[b] CRPG, UPR 2300 CNRS, 15 rue Notre Dame des Pauvres, 54501 Vandoeuvre-Lès-Nancy, France

[c] Department of Statistics, Trinity College Dublin, College Green, Dublin 2, Ireland

[d] School of Geosciences, University of Edinburgh, Drummond Street, Edinburgh EH89XP, UK

[e] Earth and Planetary Science Department, University of California Berkeley, CA 94720-4767, USA

* corresponding author. Present address: LDEO, Columbia University, Route 9W, Palisades, NY 10964, USA; Tel.: ++1 845 365 8653; Fax: ++1 845 365 8155; E-mail: schimmel@ldeo.columbia.edu

Abstract

Published cosmogenic ^{36}Cl production rates from Ca and K spallation differ by almost a factor of 2. In this paper we determine production rates of ^{36}Cl from Ca and K in samples of known age containing little Cl. Ca-rich plagioclases and K-feldspars were separated from a total of 13 samples collected on the surfaces of four basaltic lava flows at Mt. Etna (38°N, Italy) and from a trachyte lava flow at Payun Matru volcano (36°S, Argentina). Eruption ages, determined by independent methods, range between 0.4 and 32 ka. Sample site elevations range between 500 and 2500 m. Corresponding scaling factors were calculated using five different published scaling models, four of which consider paleo-geomagnetic field variations integrated over the exposure durations. The resulting five data sets were then analyzed using a Bayesian statistical model that incorporates the major inherent uncertainties in a consistent way. Spallation production rates from Ca and K, considering all major uncertainties, are 42.2 ± 4.8 atoms ^{36}Cl (g Ca)$^{-1}$a^{-1} and 124.9 ± 8.1 atoms ^{36}Cl (g K)$^{-1}$a^{-1} normalized to sea level and high latitude using the scaling method of Stone (2000). Scaling models that account for paleo-geomagnetic intensity changes yield very similar mean values (at most +4%). If the uncertainties in the independent ages are neglected in the Bayesian model, the calculated element specific production rates would be about 12% higher. Our results are in agreement with previous production rate estimations both for Ca and K if only low Cl (i.e. ≤ 20 ppm) samples are considered.

1 INTRODUCTION

In-situ cosmogenic ^{36}Cl is, along with ^{10}Be, ^{26}Al and ^{3}He, one of the most useful cosmogenic nuclides for quantifying surface processes in geomorphology (e.g. review of Gosse and Phillips, 2001). While ^{10}Be and ^{26}Al are almost exclusively measured in quartz and ^{3}He in mafic phenocrysts, ^{36}Cl is applicable to a wide range of rock types and minerals. In contrast to the other nuclides, ^{36}Cl is produced through a large range of nuclear reactions on different target elements (e.g. Fabryka-Martin, 1988, Stone et al., 1998, Gosse and Phillips, 2001). However, this complexity is a source of difficulty, because to obtain accurate ^{36}Cl exposure ages all production pathways need to be well identified, quantified and summed. Moreover, the lack of agreement between published ^{36}Cl production rates (Table 1) significantly diminishes the reliability of ^{36}Cl dating results. For this reason ^{36}Cl is often avoided in preference to other nuclides. Much progress in ^{36}Cl methodology has been made in recent years. For example, it has been shown that neither contamination by atmospheric ^{36}Cl, nor loss of in situ ^{36}Cl located within the crystal lattices is a problem (Merchel et al., 2008, Schimmelpfennig et al., 2009). Also, AMS methods have been improved and now allow accurate measurements of absolute elemental Cl concentrations by isotope dilution AMS (e.g. Ivy-Ochs et al., 2004).

At the earth's surface ^{36}Cl is mostly produced by high-energy neutron induced spallation reactions on the target elements Ca and K and to a lesser degree on Ti and Fe. The capture of low-energy neutrons by ^{35}Cl also leads to ^{36}Cl production, the rate being mainly dependent on the Cl content in the sample.

The objective of this study is to experimentally calibrate spallation production rates of ^{36}Cl from Ca and K. For this purpose, ^{36}Cl concentrations were measured in Ca- and K-rich minerals separated from well-preserved lava surfaces of known exposure history and duration. Two volcanoes were studied: Mount Etna in Italy (38°N) and Payun Matru in

Argentina (36°S). Lava flows are especially well suited for investigation of cosmogenic nuclide production rates for several reasons. Their exposure history is easily reconstructed, since for the topmost flow, the exposure age is equal to the formation age (under the assumption of zero-erosion); there are several independent methods to determine formation ages; and erosion conditions can be controlled by close examination of characteristic surface features.

The target element content of the rock material plays a crucial role in determining the suitability of a particular lava flow for reliable and accurate production rate calibration. In particular, ^{36}Cl production via the ^{35}Cl(n,γ)^{36}Cl pathway (low-energy neutron capture) is difficult to parameterize due to the complex factors affecting the distribution of low-energy neutrons at the land/atmosphere interface (Phillips et al., 2001, Schimmelpfennig et al., 2009). Therefore we used mineral separates with very low Cl contents. Another advantage of the use of minerals from Mt. Etna and Payun Matru lavas is that this suite of samples is characterized by contrasting Ca and K concentrations, which makes it possible to derive both production rates in one calibration exercise.

In order to compare calibration production rates determined at different locations in surfaces of different age, it is necessary to scale the results to a common reference place and time, typically sea level, high latitude (SLHL) at the present time. The same scaling method then allows the calibrated SLHL production rates to be back-scaled to any sample site on Earth. Balco et al. (2008) point out that the calibrated SLHL production rates must be scaled in the same way that they were originally calculated. In this study we do not seek to assess the validity of the different published scaling methods, therefore we calculate and compare the SLHL ^{36}Cl spallation production rates normalized with five different published scaling methods (Stone, 2000, Dunai, 2001, Desilets et al., 2006a, Lifton et al., 2005, Lifton et al., 2008), similar to the approach in Balco et al., 2008. The main purpose is to determine the sensitivity of ^{36}Cl SLHL production rates to the choice of scaling methods.

Because of the large number of input parameters and of non-linearities in the calculation of the production rates, it is challenging to assess the extent to which each parameter influences the final production rate and its uncertainty. In this study we developed a Bayesian statistical model to address this issue. This statistical model allows taking into account the major uncertainties in the various input parameters, and provides probability distributions for the resultant production rates, which are governed by the input data and their assigned uncertainties.

After reviewing previous ^{36}Cl production rate studies, we present the methodology with a detailed description of the sample sites, the chemical protocols, the analytical results and the assigned uncertainties. In the third section we discuss the production rate calculations including all scaling methods and the Bayesian statistical analysis used. The resultant production rates for Ca and K spallation are then presented as well as the recalculated ages for the lava flows. The new production rates are compared with previous published values and the discrepancies are discussed.

- Table 1 about here -

2 PREVIOUS PRODUCTION RATE STUDIES

As shown in the compilation of previous calibration studies in Table 1, production rates from Ca range between 48.8 ± 1.7 atoms ^{36}Cl (g Ca)$^{-1}$a^{-1} (Stone et al., 1996) and 91 ± 5 atoms ^{36}Cl (g Ca)$^{-1}$a^{-1} (Swanson and Caffee, 2001). Those from K range between 106 ± 8 atoms ^{36}Cl (g K)$^{-1}$a^{-1} (Zreda et al., 1991) and 228 ± 18 atoms ^{36}Cl (g K)$^{-1}$a^{-1} (Swanson and Caffee, 2001).

A direct comparison, however, is not straightforward since the rock type, the number of samples and their chemical composition as well as the scaling model used differed from study to study. In addition, no common method was used to apportion the total ^{36}Cl production between the various production mechanisms. To give a striking example, the production rates published by Swanson and Caffee (2001) comprise the ^{36}Cl production from spallation and slow negative muon capture (see section 4.1 for details) while those by Stone et al. (1996) and Zreda et al. (1991) are pure spallation production rates corrected for the muogenic ^{36}Cl component.

Swanson and Caffee (2001) and Licciardi et al. (2008) have summarized various possible explanations for these discrepancies. These include potential problems related to characterization of the sample sites, i.e. poorly constrained exposure histories (pre-exposure, erosion) and exposure ages; the sensitivity of the local ^{36}Cl production to the temporal variability of the geomagnetic field (especially important for high elevation and low latitude sites); and uncertainties associated with the scaling method used to normalize the local production rates to the reference point at sea level and high latitude. These points are briefly outlined here and will be discussed in more detail when our own data are discussed below.

2.1 Spatial and temporal scaling

While the correct interpretation of the exposure history and the accuracy of the independent age constraint are difficult to assess, the methods used for the spatial and temporal scaling can be compared. All so far published calibration studies used the spatial scaling of Lal (1991). In the studies of Stone et al. (1996) and Phillips et al. (1996, 2001), additional corrections for temporal geomagnetic field fluctuations were applied based on the approach described by Nishiizumi et al. (1989). The calibration sites used in the various studies are dispersed over the Northern Hemisphere between latitudes of 20° and 80° and range in altitude from 10 to 3800 m. The exposure durations range between 3 ka and 55 ka. Therefore, both inaccuracies in the spatial scaling and the effect of ignoring temporal geomagnetic fluctuations could contribute to the differences in the published calibrated production rates.

The geographic location could be relevant in another way, as has been emphasized in the study of Licciardi et al. (2008), who recognized that atmospheric pressure anomalies at their sites in Iceland could explain much of the 17% higher production rate observed there compared to sites in the western US. Further discussion of spatial and temporal scaling and recently developed scaling methods is given in section 4.2.

2.2 Calibration sample composition

The presence of numerous target elements in whole rock samples makes it difficult to isolate individual production reactions, so that an underestimate of the importance of one pathway is likely to show up in an overestimate in the importance of other pathways. Licciardi et al. (2008) discuss the importance in the choice of sample composition for the ^{36}Cl extraction and the related difficulty of modeling the distribution of the ^{36}Cl contributions from the various production reactions in samples of complex composition. Although the simple composition

found in separated minerals minimizes the influence of ^{36}Cl contributions via production reactions other than the ones being calibrated, most of the published calibration studies (Zreda et al., 1991, Phillips et al., 1996, 2001, Swanson and Caffee, 2001) used whole silicate rocks of diverse composition as calibration samples. The samples used in these studies contained not only Ca and K but were also Cl rich (Cl was as high as 350 ppm in some samples). As a consequence, individual production rates from Ca, K and low-energy neutron capture on ^{35}Cl ($^{35}Cl(n,\gamma)^{36}Cl$) had to be calibrated simultaneously. This was not possible in the study of Licciardi et al. (2008) where the narrow compositional range in Iceland basalts did not allow the calibration of more than one unknown production rate. In this case, Ca was the most abundant target element in the basalts and the Cl concentrations were considered sufficiently low (29-61 ppm) that $^{35}Cl(n,\gamma)^{36}Cl$ could be regarded as a minor reaction. Therefore, these authors only calibrated the spallation production rate from Ca, and corrected for the ^{36}Cl contributions from the other production reactions using default production rates from the literature. Instead of using whole rocks, Stone et al. (1996) and Evans et al. (1997), aware of the problems related to high chlorine concentration samples, calibrated their production rates with separated minerals. In Stone et al. (1996), a Ca-feldspar with low K (0.2%) and Cl concentrations (2-5 ppm) was used to determine the spallation production rate from Ca. The resulting value is the lowest so far observed, 48.8 ± 1.7 atoms ^{36}Cl $(g\ Ca)^{-1}a^{-1}$ (Table 1). In Evans et al. (1997), high-K feldspars with Cl contents between 9 and 315 ppm were used to determine the production rate from K. To quantify the ^{36}Cl contribution due to the $^{35}Cl(n,\gamma)^{36}Cl$ reaction in the high-K feldspars, the minerals were crushed to release Cl and the related ^{36}Cl from the fluid inclusions. However, the validity and accuracy of this approach remains uncertain and might have contributed to inaccuracy in correction for the ^{36}Cl production from thermal neutrons, which accounted for up to 60% of the total production. This could explain a possible overestimation of the final production rate from K (170 ± 25 atoms ^{36}Cl $(g\ K)^{-1}a^{-1}$).

2.3 Calibration sample number

The size of a sample set and diversity of calibration sites can be of relevance to the quality of the final result. Published sample sets range widely in sampling density e.g. three samples from one single location (Stone et al., 1996), 37 samples from 2 sites (Swanson and Caffee, 2001) or 33 samples from 14 sites Phillips et al. (1996). In some cases several samples come from various elevations at the same site (e.g. Swanson and Caffee, 2001). A large dataset is statistically more robust, however, in the specific case of a production rate calibration using samples from various geographic locations and elevations, with different exposure durations increases the risk of introducing inaccuracies attached to the scaling methods. This problem is raised in Balco et al. (2009) and will be discussed in section 5.1.

3 METHODOLOGY

3.1 Sampling strategy and site descriptions

The sampling strategy in this study was designed to minimize, as much as possible, the sources of uncertainty outlined in the previous section. Our samples were thus selected to satisfy three important criteria: (1) erosion of the lava surface could be neglected or determined accurately, (2) the age of the lava flow was independently determined, and (3) abundant Ca- or K-rich phenocrysts were present in the lava. Two calibration sites were studied: Mt. Etna on the Italian island of Sicily and volcano Payun Matru in the Argentinean province of Mendoza (Fig. 1). Both volcanoes are situated at mid-latitudes, Mt. Etna in the northern and Payun Matru in the southern hemisphere, at 38°N and 36°S, respectively.

Mt. Etna is the largest active stratovolcano in Europe. The predominant recent Etnean lava types are the so-called "etnaïtes", trachybasalts and trachyandesites with abundant plagioclase, clinopyroxene, olivine, and titanomagnetite phenocrysts (Tanguy et al., 1997 and references therein). Payun Matru is part of a volcanic complex belonging to the back-arc volcanism of the Andean range in Argentina. It is characterized by a large ignimbrite emplacement and trachytic and trachyandesitic lava with sanidine, plagioclase and clinopyroxene phenocrysts (Germa et al., 2010 and references herein). Thirteen samples were collected and analyzed: 9 from pahoehoe lava surfaces of four different flows on Mt. Etna and 4 from blocks of one aa lava flow on volcano Payun Matru. The presence of lava cords as characteristic surface features of pahoehoe flows allowed on-site assessment as to the extent of surface erosion. The geographic locations of the calibration sites and the characteristics of all samples are given in Table 2.

Both volcanoes have been tectonically stable for the time considered in this study, which implies that samples taken from the selected sites have not been subject to altitudinal variations (Rust and Kershow, 2000, Baldauf et al., 2007).

Temporary snow cover cannot be excluded at any of the sampling sites. However, because snow records do not exist for the exposure durations under consideration and any estimates would have great uncertainties, we do not calculate any snow correction, but do discuss the possible implications below.

- Table 2 about here –

- Fig. 1 about here -

Sampling sites at Mount Etna:

Note that in the following all uncertainties refer to 1σ, the standard deviation.

Historical Flow

The Historical Flow is situated on the northern flank of Mt. Etna between 2300 m and 1000 m altitude. The eruption of this flow is historically recorded between 1614 and 1624 A.D. (Tanguy et al., 1997 and references therein). One sample (HF1) was collected in the year 2007. Its age thus lies between 383 and 393 years. Due to the very young age the pahoehoe flow tops are perfectly preserved (Fig. 2a).

Solicchiata Flow

Five samples were collected at 4 different altitudes of this flow (SO1, SO2, SO3, SI3, SI40, Fig. 2b), which is located on the lower northern flank of Mt. Etna between 1200 m and 500 m. Only well-preserved surfaces showing minimal indications of erosion were sampled.

Originally, we sampled this flow for our production rate calibration assuming that the eruption age was well constrained based on Blard et al. (2005). A thorough examination of the study from which Blard et al. deduced their age (Branca 2003) led us to the conclusion that the age of this flow is only constrained by two tephra layers that have been dated by conventional radiocarbon ages of charred material at 3930 ± 60 and 15050 ± 70 ^{14}C BP years (Coltelli et al., 2000). We converted these uncalibrated radiocarbon ages into calibrated calendar ages using the program CALIB 5.0 (Stuiver and Reimer, 1986) yielding 4375 ± 76 years for the younger limit and 18350 ± 140 years for the older limit. We acknowledge that this large time range is not ideal for calibration purpose but we fully take into account this uncertainty with the Bayesian approach (see Electronic Annex section A.2).

Piano della Lepre

This site is located at an altitude of 2070 m on the southern shoulder of the "Valle del Bove" collapse structure in the southeastern part of the volcano. Sample SI43 was taken at the top of a 300 m high cliff (sloping at 70°) from a “fossil”-exposed surface (Fig. 3c). It was covered by a younger 250 cm thick overlying flow and was originally sampled for a paleoaltimetry study (Blard et al., 2005, Schimmelpfennig et al., 2009). Pahoehoe features could be distinguished on the surface of the fossil-exposed flow, indicating insignificant erosion during exposure. The overlying flow was covered by up to 50 cm of ash and therefore not suitable for sampling. The formation ages of this flow and that of the overlying flow were dated by K-Ar at 20 ± 1 ka and 10 ± 3 ka, respectively (Blard et al., 2005). The exposure time of sample SI43 can be determined by deducting the formation age of the younger flow from the formation age of the older flow, resulting in 10.0 ± 3.2 ka.

^{3}He was measured in a sample of the cliff some meters below sample SI43, and the absence of any cosmogenic ^{3}He component (Blard et al., 2005) implies a rapid retreat of the cliff wall and therefore negligible recent exposure to cosmic radiation.

La Nave Flow

The La Nave flow is situated at the margin of the northwestern flank of Mt. Etna between 1200 m and 700 m altitude. Two samples (SI41 and SI29) were taken from pahoehoe flow tops (Fig. 2d) at altitudes of 820 m and 830 m, respectively.

Blard et al. (2005) recorded 3 age determinations for this flow, 32 ± 4 ka and 33 ± 2 ka from K-Ar dating at two different locations, and 32 ± 2 ka obtained by thermoluminescence. From these three ages, the mean age, weighted by the inverse variances, is calculated (Taylor, 1997). The resulting weighted mean age and standard mean error of the La Nave flow is 32.4 ± 1.3 ka. However, ^{3}He measurements on 2 samples of the flow (Blard et al., 2006) yield significantly younger zero erosion exposure ages (25.4 ± 1.2 ka using a production rate of 128 ± 5 atoms ^{3}He (g pyroxene)$^{-1}$a^{-1}, Blard et al., 2006 and the scaling model of Stone, 2000), indicating that this flow has most probably been eroded. Although the surface shows distinguishable pahoehoe cords suggesting erosion is negligible, it is possible that sublayers exist within the lava flow. One of these sublayers could have been removed by erosion, the newly exposed layer underneath appearing pristine.

To estimate the erosion rate, the cosmogenic ^{3}He concentration measured in clinopyroxenes of sample SI41 (Blard et al., 2006) was used. Since samples SI29 and SI41 were collected in close proximity (150 m apart from each other) and have indistinguishable ^{3}He (Blard et al., 2005) and ^{36}Cl concentrations (Table 4), we assume that both samples experienced the same erosion rate.

The erosion rate ε was obtained by numerical solution of the following equation:

$$[^{3}He] = \frac{Q_s \; S_{el,s} \; PR(^{3}He) \; \Lambda_f}{\rho \; \varepsilon}\left(1 - exp\left(-\frac{\rho \; \varepsilon \; t_{expo}}{\Lambda_f}\right)\right) \qquad \text{Eq. 1}$$

where $[^3He]$ is the measured cosmogenic ^{3}He concentration, (5.27 ± 0.25) x 10^6 atoms ^{3}He g^{-1}; Q_s is the sample thickness integration factor (Schlagenhauf et al., 2010), with a value of 0.89; $S_{el,s}$ is the scaling factor, correcting for spatial and temporal variations of the production rate (Table 3); $PR(^3He)$ is the production rate of ^{3}He in olivines and clinopyroxenes normalized to sea level and high latitude, for which the value 128 ± 5 atoms ^{3}He $g^{-1}a^{-1}$ is used (Blard et al., 2006); Λ_f is the apparent fast neutron attenuation length with a value of 177 ± 2 g cm^{-2} (Farber et al., 2008); t_{expo} is the independently determined exposure duration of 32.4 ± 1.3 ka; and ρ is the density of the whole basaltic rock sample (2.52 g cm^{-3}). Assuming a lower attenuation length (160-145 g cm^{-2}) would reduce the erosion rate estimation by 10-20%.

To calculate the scaling factor $S_{el,s}$, five different scaling methods were applied according to section 4.2. The resulting five erosion rates are between 11.1 and 4.1 mm/ka (Table 3).

The relative uncertainties in each of these erosion rates are estimated at about 30% from a sensitivity test because ε cannot be solved for analytically from Eq. 1 and thus standard error propagation cannot be applied. The test accounts for the uncertainties in the independent age constraint t_{expo} (±4%, 1σ) and in the SLHL production rate $PR(^3He)$ (±4%, 1σ) as follows: values for the erosion rate ε were recalculated replacing t_{expo} and $PR(^3He)$ in Eq. 1 with all possible combinations of their confidence interval bound values (x - 2σ and x + 2σ). These bound values are 29.8 ka and 35.1 ka for t_{expo} and 118 and 138 atoms ^{3}He $g^{-1}a^{-1}$for $PR(^3He)$. The lowest and highest resulting values for ε give an idea of the limits of the confidence interval (2σ) of the mean erosion rate (~ ±60%), from which the standard deviation was derived (~ ±30%).

Blard et al. (2008) calculated the erosion rate for the same flow at a site located 6 km away from our samples to be about 13 mm ka^{-1}, as inferred from the difference between the ^{3}He and the K-Ar ages. This value is similar to our estimation. For the calculation of the SLHL ^{36}Cl

production rates, each scaling dependent erosion rate from Table 3 is used consistently with the 5 scaling methods.

- Fig. 2 about here -

- Table 3 about here -

Sampling sites at volcano Payun Matru:

The four samples were collected from well-preserved aa-block surfaces belonging to a flow located on the northern flank of the volcano, at altitudes of 2290 m and 2490 m. Blocks protrude 50 - 70 cm above the ground, are at least 50 cm wide and up to a few meters long (Fig. 3). Only blocks preserving intricate surface features, indicating insignificant erosion were sampled. Temporal snow cover in the winter months is possible, though strong winds will remove snow from protruding blocks. Moreover, those strong winds also prevent a long-term cover of the blocks with ash from later eruptions.

Germa et al. (2010) performed two K-Ar age determinations on a sample (94AE) of this flow yielding 15 ± 1 ka and 16 ± 2 ka giving a weighted mean of 15.2 ± 0.9 ka.

Payun Matru is located near the Andes, where abnormal atmospheric pressure effects could have a significant impact on cosmogenic nuclide production. However, mean annual pressure observations at the meteorological station nearest to Payun Matru, Malargue and San Rafael, (http://dss.ucar.edu/datasets/ds570.0) do not indicate any anomalies. The atmospheric pressure at station San Rafael normalized to sea level and averaged over the years 1971 to 2004 is 1013.7 ± 1.7 mbar (standard atmospheric sea level pressure is 1013.25 mbar). We assume that the present day pressure conditions are representative for the climate of the present interglacial.

- Fig. 3 about here -

3.2 Physical and chemical sample preparation

Sample preparation was conducted at CEREGE, Aix en Provence, France, and at the School of Geosciences, University of Edinburgh, UK. Pieces of uncrushed bulk rock from each lava flow were sent to the Service d'Analyse des Roches et des Minéraux (SARM) at Centre de Recherches Pétrographiques et Géochimiques (CRPG), Nancy (France) for bulk composition analysis (section 3.3). Dry rock densities were determined for each sample with pieces of uncrushed bulk rock (Table 2). Whole rock samples were then crushed and sieved to select grain size fractions between 100 µm and 1400 µm (Table 4). Separation of the feldspar minerals relied exclusively on magnetic methods, since the feldspar phenocrysts are the only non-magnetic components in the lavas. In a first step, the most magnetic grains were taken off with a strong hand magnet. Then, the less magnetic fractions were progressively removed with a Frantz magnetic separator.

The chemical extraction of ^{36}Cl (in the form of silver chloride) for AMS measurement was conducted at CEREGE. Samples consisting of feldspar grains weighing between 9 g and 325 g were first washed with MilliQ water in closed HDPE bottles for several hours on a shaker table. Then, they were etched in HDPE bottles shaken overnight in an HF (40%)/HNO_3 (2M) mixture (volume ratio 1:2) calculated to dissolve about 20% of the sample. Samples PM06-24 and PM06-26 were etched with HF and HNO_3 at the School of Geosciences, University of Edinburgh, UK to dissolve 20-30% of the grains. After this first step, any groundmass adhering to the feldspar grains should have been removed, which was verified under the binocular microscope. Moreover, potential contamination by atmospheric ^{36}Cl can totally be excluded after this rigorous leaching procedure (Merchel et al., 2008). An aliquot of 2 g was taken from the etched grains for analysis of the chemical composition at SARM (CRPG, Nancy, France). The remaining sample grains were dissolved with an excess amount of the HF/HNO_3 mixture by shaking overnight. After adding the acid mixture, the sample was spiked with approximately 1.5 mg of chloride enriched in either ^{37}Cl or ^{35}Cl (Oak Ridge National Laboratory). After complete dissolution of the grains, the solutions were centrifuged to separate the supernatant from any remaining slurry in suspension and from the fluoric cake formed during the dissolution reaction. AgCl was precipitated by adding $AgNO_3$. This first precipitate was re-dissolved in dilute NH_4OH, and, in order to reduce the isobaric interferences of ^{36}S during the ^{36}Cl AMS measurements, $Ba(NO_3)_2$ was added to precipitate $BaSO_4$ and $BaCO_3$. The AgCl was again precipitated from the resulting solution by acidification with HNO_3 and collected by centrifugation. This final precipitate was rinsed and dried and finally ^{36}Cl and Cl were measured at the LLNL-CAMS. AgCl yields, including carrier and natural Cl, accounted for 3 to 6 mg. This corresponds to 52% to 84% of the maximum possible AgCl yield.

Several blanks were prepared to survey possible contamination during the chemical extraction procedure and to correct sample measurements for laboratory sources of ^{36}Cl and Cl.

Both ^{36}Cl and Cl concentrations of a sample can be determined simultaneously from one AMS measurement by using an isotope dilution AMS technique. For this, a spike with a ^{35}Cl/^{37}Cl ratio different from the natural ratio (=3.1271) and with a known Cl concentration is added to the sample during the dissolution procedure. The ^{35}Cl/^{37}Cl ratio of the spike is guaranteed by Oak Ridge National Laboratory. The principle of isotope dilution for ^{36}Cl and Cl measurements is explained in detail in Ivy-Ochs et al. (2004) and Desilets et al. (2006b).

The details of how ^{36}Cl and Cl concentrations are derived from isotope ratios measured by AMS and the associated blank correction can be found in Schimmelpfennig (2009) and Schlagenhauf et al. (2010).

Sample SI43 was dissolved in an eight-step sequential dissolution experiment (details in Schimmelpfennig et al., 2009). ^{36}Cl and target element concentrations were determined for each dissolution step. The first three dissolution steps correspond to a removal of 25% of the initial grain weight and are similar to the etching performed on the other samples. For this calibration study, the measurements of steps 4 to 8 are included in the dataset due to their very low Cl content and are considered as four individual measurements since their ^{36}Cl concentrations depend on the target element concentrations, which vary through the dissolution process (see Table 4). The HF used to dissolve sample SI43 (Chimie-Plus Laboratories reagent grade "pure") contained non-negligible amounts of Cl and ^{36}Cl. Blank corrections of the measurements of sample SI43 therefore took account of the amount of acid used. For details see Schimmelpfennig et al. (2009).

Replicate analyses were performed for samples SI29 (two different grain sizes), PM06-31 and PM06-32 (two splits of each sample) in order to check the reproducibility of the chemical ^{36}Cl extraction.

3.3 Analytical measurements

^{36}Cl and Cl concentrations were determined at the Lawrence Livermore National Laboratory FN accelerator mass spectrometer (LLNL-CAMS) facility. Isotope dilution, using either ^{37}Cl- or ^{35}Cl-enriched carrier (^{35}Cl/^{37}Cl = 99.90%, ^{37}Cl/^{35}Cl = 98.21%), allowed the determination of both concentrations (^{36}Cl and Cl) simultaneously. ^{36}Cl/^{35}Cl and ^{36}Cl/^{37}Cl ratios were normalized to a ^{36}Cl standard prepared by K. Nishiizumi (Sharma et al., 1990). Also the stable ratio ^{35}Cl/^{37}Cl was normalized to this standard assuming the natural ratio of 3.127. Table 4 shows the measured ratios and their uncertainties. The precision of the ^{35}Cl/^{37}Cl ratios is 1% or less (standard deviation of repeated measurements), except for samples SO3 (5%) and SI41 (14%). The precision of the ^{36}Cl/^{35}Cl and ^{36}Cl/^{37}Cl ratios ranges between 2% and 4%.

Blank $^{36}Cl/^{35}Cl$ and $^{36}Cl/^{37}Cl$ ratios range between 0.9 x 10^{-14} and 1.3 x 10^{-14}. Blank corrections were done by deducting the number of atoms ^{36}Cl and Cl measured in the blanks from those measured in the samples. ^{36}Cl contents in the blanks account for 29% to 5% of measured sample ^{36}Cl (Table 4). In the case of the measurements of sample SI43, the samples were additionally corrected according to the amount of acid used to dissolve the grains, also in terms of number of atoms ^{36}Cl and Cl (section 3.2 and Schimmelpfennig et al., 2009). The resulting ^{36}Cl and Cl concentrations for all samples are listed in Table 4.

Chemical compositions were analyzed at the SARM (CRPG, Nancy, France). Major elements in the minerals and in the bulk rock were determined by ICP-OES and trace elements in the bulk rock by ICP-MS, except Li (atomic absorption), B (colorimetry), H_2O (Karl Fischer titration) and Cl (spectrophotometry). For the bulk rock analyses, pieces of whole rock were kept aside before crushing the samples (section 3.2). Concentrations of the major elements and of H, Li, B, Sm, Gd, U, Th and Cl in the bulk rocks are necessary for calculating the low-energy neutron distributions at the land/atmosphere interface. These concentrations are listed in the Electronic Annex (Table A.1). Aliquots of the etched feldspar grains, taken before their complete dissolution (section 3.2), served for the analysis of the ^{36}Cl target element concentrations (Ca, K, Ti and Fe). These concentrations and the Cl contents in the minerals, determined by isotope dilution during AMS measurements, were used to calculate the ^{36}Cl production from all production mechanisms (section 4.1) in the dissolved samples. Results of the compositional analysis, including the concentrations of ^{36}Cl and of the target elements Cl, Ca, K, Ti and Fe are listed in Table 4.

^{36}Cl concentrations range between 0.5×10^4 and 58×10^4 atoms $(g\ sample)^{-1}$. Cl concentrations in the Etna minerals range between 1 ppm and 6 ppm, Ca concentrations between 6.6% and 8.9% and K concentrations between 0.29% and 0.58%, while in the Payun Matru minerals Cl accounts for 6 ppm to 14 ppm, Ca for 0.55% and K for 5.2% to 5.4%. Ti does not exceed 0.06% and Fe is a maximum 0.59% in the calibration minerals.

As shown in Fig. 4, the large differences in ^{36}Cl concentrations are due to the variations in the prevailing target element concentrations, in the exposure duration, and in the elevation of the samples. Replicates on splits of the same sample show very good reproducibility, both in fractions of the same grain size (PM06-31 and PM06-32, the standard deviations of the means are ±0.3% and ±3%, respectively) and of different grain sizes (SI29, the standard deviation of the mean is ±1%) (section 3.2).

- Table 4 about here -

- Fig. 4 about here -

4 PRODUCTION RATE CALIBRATION APPROACH

4.1 Calculated in-situ ^{36}Cl production

The measured ^{36}Cl concentration in a sample corresponds to the sum of the ^{36}Cl contributions originating from various nuclear reactions. The major cosmogenic production reactions are spallation of Ca and K and capture of thermal and epithermal neutron (hereafter low-energy neutrons) by ^{35}Cl (^{35}Cl(n,γ) ^{36}Cl). The relative importance of the ^{35}Cl(n,γ)^{36}Cl pathway depends directly on the Cl concentration, and indirectly on the major elements and the trace elements H, Li, B, Sm and Gd that compete with Cl for absorbing the low-energy neutron flux in the sample. Minor contributions are made by capture of slow negative muons by Ca and K (Stone et al., 1998) and by spallation of Ti and Fe (Masarik, 2002, Fink et al., 2000, Stone, 2005). Additionally, radiogenic ^{36}Cl results from ^{35}Cl(n,γ)^{36}Cl, the neutrons being produced by spontaneous fission of ^{238}U and as a secondary product during the decay series of U and Th.

In a sample, the ^{36}Cl production depends on the target element concentration and on several other factors such as chemical composition, elevation, geomagnetic field, erosion, overburden and other factors.

The composition of our calibration samples (Table 4 and Fig. 5) indicates that ^{36}Cl is almost exclusively produced from the two target elements Ca and K. To gauge the relative ^{36}Cl contributions from the various production mechanisms, each was calculated using the ^{36}Cl calculation spreadsheet in Schimmelpfennig et al. (2009) based on the ^{36}Cl spallation production rates from Ca by Stone et al. (1996) and from K by Evans et al. (1997) as default values (Table 5). According to these calculations, spallation reactions on Ca and K account for 87% to 93% of total production in the Etna minerals and for 95% to 97% in the Payun Matru minerals. The low Cl concentrations in all minerals result in a small ^{36}Cl contribution of < 3.5% from low-energy neutrons and < 0.1% from radiogenic ^{36}Cl production (not listed).

The next most important production mechanism is slow negative muon capture on Ca and K, which contributes between 2% and 10% of the total ^{36}Cl inventory in the minerals (Table 5). In surface samples, the contributions from muons and spallation cannot be differentiated, since the respective nuclear reactions are on the same target elements, Ca and K.

In the following, we present the calculations on which the calibration is based. Readers are referred to the appendix of Schimmelpfennig et al. (2009) for a detailed compilation of all equations, which were adapted to the specific case of ^{36}Cl extraction from separated minerals (based on Gosse and Phillips, 2001, Fabryka-Martin, 1988).

The total measured ^{36}Cl concentration [atoms ^{36}Cl g^{-1}] in a sample corresponds to the total site- and sample-specific ^{36}Cl production from all above-mentioned reactions integrated over the exposure time. To isolate the two unknown spallation production rates PR_{Ca} and PR_{K}, [atoms ^{36}Cl (g target element)$^{-1}$a^{-1}] the relation can be written as:

$$[^{36}Cl] = A \times PR_{Ca} + B \times PR_{K} + C \qquad \text{Eq. 2}$$

with

$$A = S_{el,s}\ S_T\ Q_s\ [Ca]\ d_s\ t_{cosm,s} \qquad \text{Eq. 3}$$

and

$$B = S_{el,s}\ S_T\ Q_s\ [K]\ d_s\ t_{cosm,s} \qquad \text{Eq. 4}$$

and

$$\begin{aligned} C = & S_{el,s}\ S_T\ Q_s\ (P_{Ti} + P_{Fe})\ t_{cosm,s} + S_{el,s}\ S_T\ D\ d_s\ t_{cosm,s} \\ & + S_{el,s}\ S_T\ J_{Q,eth}\ d_{eth}\ t_{cosm,eth} + S_{el,s}\ S_T\ J_{Q,th}\ d_{th}\ t_{cosm,th} \\ & + S_{el,s}\ S_T\ E\ d_\mu\ t_{cosm,\mu} + S_{el,\mu}\ S_T\ Q_\mu\ P_\mu\ t_{cosm,\mu} + P_r\ t_r \end{aligned} \qquad \text{Eq. 5}$$

with the subscripts *s* for spallation, *eth* for epithermal and *th* for thermal neutron capture by ^{35}Cl, μ for direct capture of slow negative muons and *r* for radiogenic production. $S_{el,x}$ are the scaling factors for spallation and slow negative muon reactions, which correct the production rates for the geographic location, elevation and for temporal variations mainly due to fluctuations in the geomagnetic field (section 4.2). The scaling factor for spallation reactions $S_{el,s}$ is also applied for the low-energy-neutron reactions. S_T is the correction factor for shielding from the surrounding topography. S_T is 1 for all samples in this study, as no shielding correction was required. Q_x are the sample thickness integration factors. [Ca] and [K] are the concentrations of Ca and K, respectively, in the dissolved sample [wt%]. d_x are the depth reference factors for the respective

reaction types (Schimmelpfennig et al., 2009, Schlagenhauf et al., 2010). $t_{cosm,x}$ are the time factors for the respective cosmogenic reaction types including the radioactive decay of ^{36}Cl and the erosion rate:

$$t_{cosm,s} = (1 - exp(-t_{expo}\left(\lambda_{36} + \frac{\rho\varepsilon}{\Lambda_f}\right)))/\left(\lambda_{36} + \frac{\rho\varepsilon}{\Lambda_f}\right) \quad \text{Eq. 6}$$

$$t_{cosm,eth} = (1 - exp(-t_{expo}\left(\lambda_{36} + \frac{\rho\varepsilon}{L_{eth}}\right)))/\left(\lambda_{36} + \frac{\rho\varepsilon}{L_{eth}}\right) \quad \text{Eq. 7}$$

$$t_{cosm,th} = (1 - exp(-t_{expo}\left(\lambda_{36} + \frac{\rho\varepsilon}{L_{th}}\right)))/\left(\lambda_{36} + \frac{\rho\varepsilon}{L_{th}}\right) \quad \text{Eq. 8}$$

$$t_{cosm,\mu} = (1 - exp(-t_{expo}\left(\lambda_{36} + \frac{\rho\varepsilon}{\Lambda_\mu}\right)))/\left(\lambda_{36} + \frac{\rho\varepsilon}{\Lambda_\mu}\right) \quad \text{Eq. 9}$$

where t_{expo} is the exposure duration [a], λ_{36} the decay constant of ^{36}Cl (2.303 x 10^{-6} a^{-1}), ε is the constant erosion rate [cm a^{-1}], ρ the density of the sample [g cm^{-3}], Λ_i the apparent fast neutron attenuation length (177 g cm^{-2}, Farber et al., 2008), L_{eth} and L_{th} are the composition dependent epithermal and thermal neutron diffusion lengths [g cm^{-2}] (see Schimmelpfennig et al., 2009 for details), respectively, and Λ_μ is the slow negative muon attenuation length (1500 g^{-2}, Heisinger et al., 2002).

P_{Ti} and P_{Fe} are the sample-specific depth-dependent ^{36}Cl production rates from spallation of Ti and Fe [atoms ^{36}Cl (g^{-1}sample) a^{-1}], respectively. $J_{Q,x}$ are the production rate coefficients which account for sample thickness integration factors Q_x, all composition-dependent variables, SLHL production rates and parameters of all reactions. D is the second part of the calculation of $J_{Q,s}$ (see for detail Eq. 68 in Schimmelpfennig et al., 2009), and E is the first part of the calculation of $J_{Q,\mu}$ (see for detail Eq. 71 in Schimmelpfennig et al., 2009). P_r is the composition-dependent radiogenic ^{36}Cl production rate and t_r is the time factor for the radiogenic reaction including the radioactive decay of ^{36}Cl:

$$t_r = (1 - exp(-t_{form}\lambda_{36}))/\lambda_{36} \quad \text{Eq. 10}$$

where t_{form} is the formation time of the rock [a], which can be different from the exposure time, e.g. for buried surfaces like sample SI43 in this study (section 3.1).

All composition- and depth-dependent variables were calculated using the ^{36}Cl calculation spreadsheet (Schimmelpfennig et al., 2009). Their values are listed for all samples in the Electronic Annex in Table A.3. The production rates of the minor production mechanisms such as $P\mu$ were taken from the literature and are presented in Table 5.

Although the minerals were dominantly either Ca- or K-feldspars, for all rocks, production from both Ca and K was considered. For example, at Mt. Etna spallation from Ca accounts for 74-80% and K for 9% to 16%; and at Payun Matru spallation on Ca accounts for 3% and K for 92-94%. Therefore, the wide range of the Ca/K ratio, with ratios for Etna

samples that vary from 15 to 28 and for Payun samples that are about 0.1, allows calibrating the two spallation production rates simultaneously in the same calibration exercise.

- Fig. 5 about here -

- Table 5 about here -

4.2 Scaling methods

To interpret measured cosmogenic nuclide concentrations correctly, the latitude, elevation and time dependency of production rates need to be quantified accurately. This is accomplished through scaling models, which quantify this variability by calculating scaling factors that integrate the specific site latitude, altitude and time span. Several different scaling models have been published.

The first method to calculate local production rates as a function of latitude and elevation was published by Lal (1991). Stone (2000) refined Lal's method by expressing the elevation dependence in terms of atmospheric pressure. Concurrently and subsequently, Dunai (2000), Dunai (2001), Desilets and Zreda (2003), Desilets et al. (2006a), Lifton et al. (2005), Lifton et al. (2008) developed more complex methods that account for the elevation effect as a function of atmospheric depth, for the latitude effect in terms of cutoff-rigidity, and for the time dependence of the geomagnetic field intensity.

For this study, five of these methods were selected to calculate scaling factors for each calibration sample site: Stone (2000) (St), Dunai (2001) (Du), Desilets et al. (2006a) (De), Lifton et al. (2005) (Li05) and Lifton et al. (2008) (Li08). The citations will hereafter be substituted by the abbreviation in brackets. The characteristics of each scaling method are described in Table 6 with the corresponding geomagnetic field model and reference source used. It is not in the scope of this paper to discuss the validity of these models, but it is important to stress that these various scaling methods do exhibit significant differences in certain geographic regions and periods of time and that mixing them can introduce significant bias (Balco et al., 2008).

For that reason we have normalized the production rate derived from our data to SLHL at the present time using each of the five different scaling models. Thus future applications using our reference production rate need not to be limited to any particular scaling model. The

scaling factors derived for spallation and muon-induced production at each sampling site can be found in detail in the Electronic Annex (Table A.2) and are displayed in Fig. 6 normalized to the Stone (2000) scaling factor. Absolute values range between 1 and 6 due to the variation in altitude and exposure duration of the sites (the latitude is for all sites similar, Mt. Etna 38°N, Payun Matru 36°S).

The spallation scaling factors $S_{el,s}$ from the different methods seem to differ most strongly as a function of the time span over which the scaling factors are integrated, and less as a function of the altitude. Spallation scaling factors for flows younger than 10 ka vary more strongly (up to 23%) than for older flows (up to 15%), which is mainly because the geomagnetic field intensity records differ before and after 10 ka. For $t < 10$ ka, the fluctuations of the geomagnetic field have a higher resolution and are less effectively averaged out for flows in this time range. This is most striking for the historic flow, which has a very short exposure duration (< 400 years). It should also be noted that geomagnetic fluctuations after AD 1950 are not incorporated in the scaling calculations (Balco et al., 2008), which might have an effect on the historical flow.

At Mt. Etna, spallation scaling factors differs by at most 23% between the models due to the spread in ages and altitudes, while at Payun-Matru the five scaling methods yield more similar scaling factors with a maximum discrepancy of 7% (Fig. 6a).

Li05 and Li08 scaling models generally yield the lowest spallation scaling factor values while for the other scaling methods no systematic tendency is observed.

The muon scaling factors $S_{el,\mu}$, on the other hand, show a systematic offset of about 10% between St, Du and De. In addition, Li05 and Li08 muon scaling factors display a different altitude dependence compared to the others models. This can be explained by the fact that in Li05 and Li08 the muon attenuation coefficient in the atmosphere is calculated with a polynomial, fitted on the basis of muon monitor data, while the other methods use linear functions to calculate the muon attenuation coefficient.

It has to be stressed that we are calibrating *spallation* production rates and the $S_{el,\mu}$ are not expected to have a significant influence on the spallation production rate results.

Balco et al. (2008) give an overview of the relative differences in calculated cosmogenic ^{10}Be and ^{26}Al exposure ages, when scaled with the different methods, as a function of the latitude, the elevation and the exposure duration. Temporal variations and related differences in the scaling factors for varying exposure durations have the greatest impact at low latitudes, where changes in paleomagnetic field strength are most important. Scaling factors of the different methods are most similar at moderate elevations and diverge most strongly at high elevations but also at very low latitudes. For our study, samples were taken at mid-latitude and at a moderate elevation range (530-2500m), where the scaling is not so much affected by the discrepancies highlighted in Balco et al. (2008).

- Table 6 about here -

- Fig. 6 about here -

4.3 Statistical approach and uncertainties in the dataset

A fundamental drawback in the numerical and statistical methods of previous calibration studies has been the lack of a consistent approach for both inverting the measured data to infer production rates and for incorporating the uncertainties of the dataset. In contrast to standard regression or least square methods, the Bayesian statistical model (e.g. Gelman et al., 2004 and references therein) allows the uncertainties with different ranges and distributions (uniform or Gaussian) to be included in a self-consistent manner. In particular, the large uncertainty in the Solicchiata independent age as well as the poorly constrained erosion rate of the La Nave can be taken into account.

Following Gelman et al. (2004), "Bayesian inference is the process of fitting a probability model to a set of data and associated uncertainties and summarizing the result by a probability distribution on the parameters of the model…". This approach has already been successfully applied in archeology, paleontology and in paleoseismology (e.g., Buck and Bard, 2007, Hilley and Young, 2008). In geochronology the approach has been used to reconcile and combine ages originating from various methods (Muzikar and Granger, 2006).

The advantage of using a Bayesian approach is that the uncertainty in each parameter can be integrated in the model as a probability distribution, which is called the "prior distribution". The inferred result is the "posterior distribution" which is expressed as the probability distributions of those parameters deduced from the combination of the model structure and the priors. The Bayesian model, associated inference and algorithm used are detailed in the Electronic Annex section A.2.

In the following section we detail both the uncertainties that were included in the inversion and those that were small enough to be ignored in the final calculation. The impacts on the calibration of the various uncertainties considered in the calibration were tested by running the statistical algorithm several times, first including all selected uncertainties, then only the

uncertainties in the independent age constraints and finally without any uncertainty, taking the mean values of the distributions of each of the five independent ages. For the Historical Flow and the Solicchiata flow, the center between the minimum and maximum value of their uniform distributions were used as independent age value.

Uncertainties in the independent ages

The time factors, $t_{cosm,x}$ (Eq. 6 – 9), are related to the independent age, t_{expo}, as long as the exposure duration is relatively short (<< steady state), as is the case in this study. Two of the five lava flows have poorly constrained independent exposure durations. The Solicchiata flow erupted between 4.4 ka and 18.4 ka and the Piano della Lepre surface (sample SI43) has a calculated exposure time with a 32% uncertainty.

The other three flows have age constraints with uncertainties between 1.3% and 6%.

Uncertainty in the erosion rate

The time factors $t_{cosm,x}$ also depend on the erosion rate which could have a significant influence on the final results. For the La Nave flow, exposed for 32 ka, there is a 17% difference in the time factor between considering a constant erosion rate of 10 mm/ka and ignoring erosion completely. However, although the uncertainty in the erosion rate is high (30%) (Section 3.1), the final calibration results are probably not strongly affected by this uncertainty, since we have included erosion only for the La Nave flow in our Bayesian model. For most of the flows, which are relatively young, the effect of erosion would be quite small.

Uncertainty in the production from slow negative muon capture

The predicted ^{36}Cl contribution from slow negative muon capture accounts for 2 to 10% of the total ^{36}Cl inventory (Table 5). In the calibration model, the total ^{36}Cl inventory is corrected for this contribution to accurately determine the production rates only from spallation (see Eq. 2 – 5). The uncertainty in the calculated production rate from muon capture P_μ is estimated at 25%. This is because Gosse and Phillips (2001) associated an error of ±25% to the calculation of the compound factor f_c using the Fermi-Teller Z-law (Charalambus, 1971). f_c is a poorly known factor in the calculation of the ^{36}Cl yield per muon stopped by the target elements (Eq. 3.44 in Gosse and Phillips, 2001). Propagating the uncertainty in f_c and minor uncertainties in other factors into P_μ results in an uncertainty of ~25% for P_μ.

Analytical and other uncertainties

We also consider the analytical uncertainties in the measured ^{36}Cl concentrations N_{36} (σ_{analyt}), which range between 2% and 7%. Note that these uncertainties take account not only of uncertainties related to AMS measurements but also include the uncertainties in the chemical process blanks. Through standard error propagation the uncertainty in the final ^{36}Cl concentration increases the higher the relative blank correction (Table 4).

The uncertainties of the other parameters in the dataset either have much smaller magnitudes than those stated above or will not significantly affect the results of the calibration. Errors in the concentrations of Ca in the Ca-rich samples and of K in the K-rich samples are typically 2% or less (Table 4). Only the four measurements of sample SI43 have Ca concentrations with higher uncertainties (5-26%), but this is due to the special dissolution procedure applied to this sample and the mass balance calculations to determine target element concentrations (for details see Schimmelpfennig et al., 2009). The uncertainties in the Cl concentrations can be as high as 80% for samples with Cl contents <3 ppm (Table 4). However, since the Cl contents in all samples are very low, the calculated ^{36}Cl contributions due to Cl are

insignificant in the total ^{36}Cl inventory (max. 3.5%, Table 5). The calibration results are therefore insensitive to the uncertainties in the Cl concentrations.

The sensitivity to errors in other components such as the attenuation length for fast neutrons (Λ_f), the rock density and the sample thickness were tested in the ^{36}Cl calculation spreadsheet using reasonable error estimates (~10%) and were found to have insignificant impacts in the resulting exposure ages and are therefore expected to have insignificant impacts in the calibration results as well.

Uncertainties in the scaling factors were not calculated, because they are hard to estimate due to the complexity of their determination (Desilets et al., 2006a). Instead, we independently calibrate the ^{36}Cl production rates with five different scaling methods to illustrate the sensitivity of the results to the choice of the method.

5 RESULTS AND DISCUSSION

5.1 New spallation production rates from Ca and K

Fig. 7 shows the posterior distributions of the spallation production rates PR_{Ca} and PR_K resulting from the dataset scaled to SLHL according to St scaling model (the distributions of all the other scaling models can be found in Fig. A.1 in the Electronic Annex). The highest probability corresponds to the mean value for the production rate that best explains all the data. The geometry of the distributions is in all cases close to normal. Table 7a summarizes the results from all five datasets at SLHL. The mean values of PR_{Ca} are very similar, ranging between 41.6 and 44.0 atoms ^{36}Cl (g Ca)$^{-1}$a^{-1}, and those of PR_K have a wider range between 124.0 and 135.1 atoms ^{36}Cl (g K)$^{-1}$a^{-1} with standard deviations on the order of 10% for PR_{Ca} and 7% for PR_K. If the uncertainty in both the erosion rate of the "La Nave" flow (±30%, 1σ) and the muon production rate (P_μ) (±25%, 1σ) are not considered, the standard deviation of PR_{Ca} decreases to about 8% whilst mean PR_{Ca} and PR_K, and the uncertainty in PR_K are unchanged (Table 7b). Therefore, considering only uncertainties in independent ages, does not change the resulting spallation production rate mean values but does reduce their uncertainties by about 2%. When all uncertainties are neglected, the resulting mean values for PR_{Ca} increase between 4% and 12% depending on the scaling model, while PR_K remains little changed (Table 7c). The standard deviations for PR_{Ca} and PR_K are also lowered (~5% for PR_{Ca} and ~2% for PR_K). This result illustrates that Bayesian analysis mutes but does not ignore the effect of the large uncertainty on the independent age of the Solicchiata flow.

PR_K is primarily constrained by the four Payun Matru sanidine samples with a ^{36}Cl contribution from spallation on K that accounts for about 93% of the total (Table 5). Similarly, PR_{Ca} is mainly constrained by the Mt. Etna plagioclase but here the contribution from K is still significant (9% - 16%). Hence, the well-defined independent age of the Payun

Matru flow is the reason why ignoring uncertainties on the independent ages does not affect the PR_K value. On the other hand, disregarding age uncertainties yields a different mean for the calculated PR_{Ca} probably due to the poor constraint of the independent age of the Solicchiata flow, which constitutes one fourth of the data set. Moreover, while the SLHL PR_{Ca} values with or without uncertainties in the independent ages agree within standard deviations when using the St, Du and De scaling models, this is not the case with Li05 and Li08 models.

In summary, the relatively large uncertainties in our production rates originate mainly from the uncertainties in the independent ages.

With respect to the various scaling models, PR_{Ca} mean values are very similar with a maximum difference of 5% between the "De" version and the "Li08" version (Table 7a). This occurs in spite of the fact that differences in the spallation scaling factors at Mt. Etna reach 23% (section 4.2 and Fig. 6). On the other hand, the PR_K mean values differ by almost 8% (between “De” and “Li05”), while the differences in the scaling factors are much smaller at Payun Matru (7%) than at Mt. Etna. Thus, the observed differences in the scaling factors are almost averaged out in the final PR_{Ca} value over the range of elevations (500 – 2000 m) and exposure durations (388 years – 32 ka) encountered, while this is not the case for the PR_K value, which is mainly constrained by a much smaller number of samples, collected from the same flow at very similar altitudes. The tendency of the Li05 and Li08 scaling factors to be systematically lower than the others is reflected by higher resulting mean values of the production rates. However, at this point inaccuracies due to the scaling schemes, cannot be deconvoluted from errors related to the independent age.

- Fig. 7 about here -

- Table 7 about here -

5.2 Comparison to previous published production rates

The SLHL production rates determined in this study lie in the lower range of published ^{36}Cl calibrated spallation production rates. The discrepancies most probably arise from methodological differences in the manner in which the different calibrations were performed. Indeed, it can be observed that calibration studies relying on silicate whole rock, which often contain high Cl contents (up to 350 ppm), generally yield higher production rates (PR_{Ca} in Zreda et al., 1991, Phillips et al., 1996, 2001, Swanson and Caffee, 2001, Licciardi et al., 2008 ignoring corrections for abnormal pressure conditions; PR_K in Phillips et al., 1996, Swanson and Caffee, 2001). An overestimation of spallation production rates calibrated with high-Cl samples could be due to an underestimation of the ^{36}Cl production from the $^{35}Cl(n,\gamma)^{36}Cl$ pathway, as shown in Schimmelpfennig et al. (2009). The low production rates found in this study, on the other hand, are in best agreement with production rates calibrated with low-Cl samples as shown in the next paragraph.

PR_{Ca}, scaled according to Stone (2000), has a value of 42.2 ± 4.8 atoms ^{36}Cl (g Ca)$^{-1}$a^{-1} (Table 7a) and is closest to that of Stone et al. (1996) (48.8 ± 1.7 atoms ^{36}Cl (g Ca)$^{-1}$a^{-1}, Table 1), scaled with Lal (1991). These results nearly overlap at 1σ. Stone et al. (1996) used separated Ca-feldspar samples from a basaltic lava flow dated at 17.3 ka, falling in the exposure duration range of this study. The sample site is located at latitude 39°N and an elevation of 1445 m, both very similar to the spatial conditions of the Mt. Etna samples. Also the Cl content in the samples (2-5 ppm) is on the same order as that of the minerals used for this study. These methodological similarities might explain why the results are so close. The difference is that Stone et al. (1996) used only three samples from one single flow and from the same elevation, while our SLHL PR_{Ca} is calibrated from samples coming from several flows, elevations and exposure durations.

For the Mt. Etna samples we made no attempt to correct for potential snow cover because records show that snow is limited to less than 1 or 2 months per year at the altitudes of the sampling sites. However, the corresponding snow correction would be less than 5% (e.g. Benson et al., 2004, Schildgen et al., 2005) and would therefore increase PR_{Ca} insignificantly. Moreover, considering a small erosion rate (<5 mm/ka) on the Solicchiata and Piano della Lepre flows would also increase our production rate. However, our field observations of flow surface morphology do not support making any erosion correction for these two young flows (less than 15 ka). Nevertheless, if those corrections were acknowledged this would merge our production rate with that of Stone et al. (1996).

Our spallation production rate PR_K, scaled with St, has a value of 124.5 ± 8.1 atoms ^{36}Cl (g $K)^{-1}a^{-1}$ in agreement at the 1σ level with that determined by Phillips et al. (2001), 137 ± 9 atoms ^{36}Cl (g $K)^{-1}a^{-1}$, scaled according to Lal (1991) (Table 7a). The sample set in Phillips et al. (2001) consists of a series of 30 whole rocks of diverse composition, collected at numerous sites from a wide range of latitudes, longitudes, elevations and exposure durations (Phillips et al., 1996) and were used for the calibration of PR_{Ca}, PR_K and $P_f(0)$ (production rate of epithermal neutrons from fast neutrons). However, K concentrations are quite low in all samples. Only 3 samples have higher K contents than Ca contents with maximum 4.4% and 2.7% K in two samples. These two samples have the lowest Cl contents in the sample set, with 6 and 18 ppm Cl, and very low Ca (~0.02%) and probably therefore exert the strongest control on the resulting production rate from K. The exposure duration of these samples is similar (12 ka) to that of the Payun Matru samples (15 ka), but the elevation and the latitude are different (375 m and 52°N).

Evans et al. (1997) on the other hand used a K-feldpar mineral separate with Cl content ranging between 1 to 315 ppm. Samples were collected at various latitudes (38°N, 58°N) with altitude between 500 and 3600 m. The preferred value of Evans et al. (1997) of 170 ± 25 atoms ^{36}Cl (g $K)^{-1}a^{-1}$ is supported by 11 samples among which only three had chlorine

concentrations lower than 143 ppm. On a closer inspection of Figure 3 in Evans et al. (1997), we observe that two samples yield lower production rate between 110 and 120 atoms ^{36}Cl (g K)$^{-1}$a^{-1}, values that would be in agreement with our proposed production rate. Whether those samples are the ones with lowest chlorine concentration is not clear in the paper, but it is probable that high Cl concentration of all the other samples might have yielded an overestimation of the final production rate.

5.3 Recalculated ^{36}Cl ages of the Etna and Payun Matru lava flows

To assess the internal and external consistency of the whole data set, the exposure age of each individual sample and the mean exposure age for each flow are calculated according to the new calibrated ^{36}Cl production rates in two ways and compared to the independent ages. First, the statistical algorithm provides mean ages for each flow (Table 8) as posterior distributions. Secondly, the exposure ages of each sample were calculated with the ^{36}Cl calculation spreadsheet of Schimmelpfennig et al. (2009) using the production rates deduced from this calibration exercise (Table 9). Fig. 8a shows all these ages and the independent age constraints for comparison, using the St scaling method, and Fig. 8b using the Li08 scaling model. This choice was made because the new "St" production rates are among the lowest mean values, while the new "Li08" production rates are among the highest mean values. All ages from the individual samples, the mean values for each flow and the independent age are in good agreement. Only for the Historical Flow when using the St model is the exposure age fit with the expected age as poor as 2σ, while with the Li08 model it agrees within 1σ. This discrepancy is due to the huge difference between these two scaling schemes for the spallation scaling factor (Fig. 6), and probably arises from the very young age of the flow. Inaccuracies in the temporal variations of the cosmogenic nuclide production do not average out over such a short period, and the St scaling does not correct for changes in production rate

with time while Li08 model does. The statistical algorithm, on the other hand, calculates the same exposure age of 388 ± 3 years for all five scaling schemes. This is because the uniform distribution of the priors for the independent age constraint of this flow prohibits the posteriors to go beyond the limits of this closed interval.

For the least well constrained exposure age flow, the Solicchiata flow, the resulting exposure age is 7.2 ± 1.0 ka using St scaling and 8.5 ± 1.1 ka using Li08 scaling. Both ages are in agreement (1σ) and lie close to the younger limit of the independent age interval. Based on field observations of flow superpositions, Branca (2003) estimated that this flow had an eruption age younger than 7 ka (see Fig. 5 in Branca, 2003). This estimate is close to our calculated age. Also exposure ages calculated with cosmogenic ^{3}He concentrations in pyroxenes and olivines of samples SI3 and SI40 (Blard et al., 2005) yield ages in agreement with ours (5.8 ± 0.4 ka using St and 7.2 ± 0.5 ka using Li08 calculated with the production rate 128 ± 5 atoms ^{3}He $g^{-1}a^{-1}$).

The recalculated mean values of sample SI43 (Piano della Lepre flow) are higher (11.7 ± 1.1 ka St scaling and 12.7 ± 0.9 ka Li08 scaling) than the independent mean value, but lie within one standard deviation (10.0 ± 3.2 ka). For the two flows La Nave and Payun Matru, the recalculated mean values are in excellent agreement with the independent ages.

All our recalculated ages agree within uncertainties with the independent ages regardless of the scaling mode. In addition, we do not see any dependence on latitude or altitude on the resulting exposure ages for any of the scaling models. However, because of the relatively small range of elevation and latitude of our sites, our measurements are relatively insensitive to such effects. This has the advantage of yielding an accurate production rate determination independently of the chosen scaling scheme. On the other hand since we cannot evaluate the effects of the scaling models over a wide range of regional parameters, it is difficult to assess whether our production rate can be extrapolated to high latitude or to high altitude or over much longer time spans.

- Table 8 about here -

- Table 9 about here -

- Fig. 8 about here -

6 CONCLUSIONS

In order to determine ^{36}Cl spallation production rates from Ca and K, volcanic rocks containing Ca and K rich minerals with low Cl contents were sampled from flows with good independent age control. The 13 surface samples collected were located at latitude 38°N and 36°S, at altitudes between 500 and 2500 m and with ages ranging from 383 to 32,000 years. These 13 samples generated 20 measurements, which included 2 full chemical replicates and a set of 4 stepwise chemical etchings. Each of the five published scaling schemes was applied, generating five versions of the dataset. This enables users of these new production rates to calculate exposure ages according to the scaling scheme of their choice. A Bayesian statistical model developed to calculate the spallation production rates from the dataset includes *all* inherent major uncertainties in a consistent way. The resulting spallation production rates from Ca and K are, considering all uncertainties, 42.2 ± 4.8 atoms ^{36}Cl (g Ca)$^{-1}$a^{-1} and 124.9 ± 8.1 atoms ^{36}Cl (g K)$^{-1}$a^{-1} at SLHL scaled with Stone (2000). Production rate values scaled with all other scaling models are similar but there are differences of the order of 5-10%. For example, mean values of PR_{Ca} and PR_K scaled with Lifton et al. (2005) or Lifton et al. (2008) differ by almost 6-8% from those scaled with Desilets et al. (2006a). Therefore, applying PR_{Ca} and PR_K based on one scaling scheme to a surface of unknown age by using a different scaling scheme may induce a significant bias in the final result.

The relatively large uncertainties in our derived production rates are mainly due to the uncertainties in the independent age constraints of the sampled lava flows. Ignoring the uncertainty in the independent ages during the inversion of our dataset would lead to a 12% shift in PR_{Ca} but little change in PR_K. This result emphasizes the importance of performing a statistical analysis of the dataset in which all major uncertainties can be accounted for.

When comparing our production rates with previously published values from samples low in Cl (Phillips et al., 2001; Stone et al., 1996), we find good agreement for both K and Ca

production rates. Moreover, although the time spanned by our data (383 years to 32,000 years) is long and the altitude range (500-2500 m) is significant, the ages recalculated with our production rates are mostly in agreement, within uncertainty, with the independent ages. This suggests that, although there are discrepancies in the scaling methods, for our samples the uncertainties in the independent ages preclude seeing any altitude dependency.

A question that has to be addressed in future studies is whether the spallation ^{36}Cl production from the two target elements Ca and K can be scaled with the same scaling scheme, as was done in this study. ^{36}Cl is produced from K at a lower energy threshold than from Ca and therefore the altitudinal dependence on the scaling factors might be different (Desilets et al., 2006a, Michel et al., 1995). In our case, the chemical composition of our samples and their respective altitude do not allow us to evaluate this issue.

The strategy presented in this study provides a firm basis for a methodology, by which numerous measurements from widespread calibration sites can be combined with the goal of refining ^{36}Cl production rates from spallation of Ca and K. However, as long as scaling is not more accurate, it will not be possible to obtain SLHL ^{36}Cl production rates from a large data set without introducing systematic errors. The challenge remains to find good calibration sites with accurate absolute independent ages.

Acknowledgement:

This work is part of the CRONUS-EU project and is funded by the Marie Curie research network Contract No. 511927. We gratefully thank Anne-Sophie Mériaux, Jérôme Chmeleff and Carmelo Monaco for essential help concerning the choice of sample sites and during fieldwork. Xavier Quidelleur and Stefano Branca are acknowledged for providing indispensable information about the independent age constraints of the lava flows. We are grateful to Eric Gayer for physically sample preparation of two samples and to Silke Merchel for her useful support in the lab. L. Sevin, J. Marin and all the staff at SARM-CRPG are acknowledged for the compositional measurements. We are very thankful to T. Guilderson and T. Brown as well as all the staff of the CAMS-LLNL for their invaluable assistance and support for the ^{36}Cl measurements. We wish to thank Nat Lifton for providing valuable information about his scaling models. Finally, David Fink, Joe Licciardi, an anonymous reviewer and the associated editor Gregory Herzog are gratefully acknowledged for their thorough and very constructive reviews that greatly improved the manuscript.

References:

Balco G., Stone J., Lifton N. and Dunai T. (2008) A complete and easily accessible means of calculating surface exposure ages or erosion rates from ^{10}Be and ^{26}Al measurements. *Quaternary Geochronology* **3**, 174-195.

Balco G., Briner J., Finkel R. C., Rayburn J. A., Ridge J. C. and Schaefer J. M. (2009) Regional beryllium-10 production rate calibration for late-glacial northeastern North America. *Quaternary Geochronology* **4**, 93-107.

Baldauf P.E., Combina A.M., Nullo F.E. and Stephens G. (2007) Andean uplift and foreland basin formation in western Argentina, Mendoza Province, 34°30' - 35°30'S. Geological Society of America *Abstracts with Programs*, Vol. **39**, No. 6, p. 236.

Benson L., Madole R., Phillips W., Landis G., Thomas T. and Kubik P. (2004) The probable importance of snow and sediment shielding on cosmogenic ages of north-central Colorado Pinedale and pre-Pinedale moraines. *Quaternary Science Reviews* **23**, 193-206.

Blard P. H., Lavé J., Pik R., Quidelleur X., Bourlès D. and Kieffer G. (2005) Fossil cosmogenic He record from K-Ar dated basaltic flows of Mount Etna volcano (Sicily, 38°N): Evaluation of a new paleoaltimeter. *Earth and Planetary Science Letters* **236**, 613-631.

Blard P. H., Pik R., Lavé J., Bourlès D. L., Burnard P., Yokochi R., Marty B. and Trusdell F. (2006) Cosmogenic ^{3}He production rates revisited from evidences of grain size dependent release of matrix-sited helium. *Earth and Planetary Science Letters* **247**, 222-234.

Blard P. H., Bourlès D., Pik R. and Lavé J. (2008) In situ cosmogenic ^{10}Be in olivines and pyroxenes. *Quaternary Geochronology* **3**, 196-205.

Branca, S. (2003) Geological and geomorphological evolution of the Etna volcano NE flank and relationships between lava flow invasions and erosional processes in the Alcantara Valley (Italy). *Geomorphology* **53**, 247-261.

Buck C.E. and Bard E. (2007) A calendar chronology for Pleistocene mammoth and horse extinction in North America based on Bayesian radiocarbon calibration. *Quaternary Science Reviews* **26**, 2031-2035.

Charalambus S. (1971) Nuclear transmutation by negative stopped muons and the activity induced by the cosmic-ray muons. *Nuclear Physics* **A166**, 145-161.

Coltelli M., Carlo P. D. and Vezzoli L. (2000) Stratigraphic constraints for explosive activity in the past 100 ka at Etna Volcano, Italy. *International Journal of Earth Sciences* **89**, 665-677.

Desilets D. and Zreda M. (2003) Spatial and temporal distribution of secondary cosmic-ray nucleon intensities and applications to in situ cosmogenic dating. *Earth and Planetary Science Letters* **206**, 21-42.

Desilets D., Zreda M. and Prabu T. (2006a). Extended scaling factors for in situ cosmogenic nuclides: New measurements at low latitude. *Earth and Planetary Science Letters* **246**, 265-276.

Desilets D., Zreda M., Almasi P. and Elmore D. (2006b). Determination of cosmogenic ^{36}Cl in rocks by isotope dilution: innovations, validation and error propagation. *Chemical Geology* **233**, 185-195.

Dunai T. J. (2000) Scaling factors for production rates of in situ produced cosmogenic nuclides: a critical reevalution. *Earth and Planetary Science Letters* **176**, 157-169.

Dunai T. J. (2001) Influence of secular variation of the geomagnetic field on production rates of in situ produced cosmogenic nuclides. *Earth and Planetary Science Letters* **193**, 197-212.

Evans J. M., Stone J. O., Fifield L. K. and Cresswell R. G. (1997) Cosmogenic ^{36}Cl production in K-feldspar. *Nuclear Instruments and Methods in Physics Research Section B* **123**, 334-340.

Fabryka-Martin J. T. (1988) Production of radionuclides in the earth and their hydrogeologic significance, with emphasis on chlorine-36 and iodine-129. Ph.D. thesis, University of Arizona, Tucson.

Farber D. L., Mériaux A.-S. and Finkel R. C. (2008) Attenuation length for fast nucleon production of ^{10}Be derived from near-surface production profiles. *Earth and Planetary Science Letters* **274**, 295-300.

Fink D., Vogt S. and Hotchkis M. (2000) Cross-sections for ^{36}Cl from Ti at E_p = 35-150 MeV: Applications to in-situ exposure dating. *Nuclear Instruments and Methods in Physics Research Section B* **172**, 861-866.

Gelman A., Carlin J. B., Stern H. S. and Rubin D. B. (2004) Bayesian Data Analysis, 2nd Edition. *Texts in Statistical Science.* Chapman & Hall/CRC, Boca Raton.

Germa A., Quidelleur X., Gillot P. Y. and Tchilinguirian P. (2010) Volcanic evolution of the back-arc Pleistocene Payun Matru Volcanic Field (Argentina). *Journal of South American Earth Sciences* **29**, 717-730.

Gosse J. C. and Phillips F. M. (2001) Terrestrial in situ cosmogenic nuclides: theory and application. *Quaternary Science Reviews* **20**, 1475-1560.

Guyodo Y. and Valet, J. P. (2000) Global changes in intensity of the Earth's magnetic field during the past 800 kyr. *Nature* **399**, 249-252.

Heisinger B., Lal D., Jull A. J. T., Kubik P., Ivy-Ochs S., Knie K. and Nolte E. (2002) Production of selected cosmogenic radionuclides by muons: 2. Capture of negative muons. *Earth and Planetary Science Letters* **200**, 357–369.

Hilley G. E. and Young J. J. (2008) Deducing paleoearthquake time and recurrence from paleoseismic data, Part II: Analysis of paleoseismic excavation data and earthquake behavior along the Central and Southern San Andreas Fault. *Bulletin of the Seismological Society of America* **98**, 407-439.

Ivy-Ochs S., Synal H.-A., Roth C. and Schaller M. (2004) Initial results from isotope dilution for Cl and ^{36}Cl measurements at the PSI/ETH Zurich AMS facility. *Nuclear Instruments and Methods in Physics Research Section B* **223-224**, 623-627.

Korte M. and Constable C. G. (2005) Continuous geomagnetic field models for the past 7 millennia: 2. CALS7K. *Geochemistry Geophysics Geosystems* **6**, Q02H16.

Lal D. (1991) Cosmic ray labeling of erosion surfaces: in situ nuclide production rates and erosion models. *Earth and Planetary Science Letters* **104**, 424-439.

Licciardi J., Denoncourt C. and Finkel R. (2008) Cosmogenic ^{36}Cl production rates from Ca spallation in Iceland. *Earth and Planetary Science Letters* **267**, 365-377.

Lifton N., Bieber J., Clem J., Duldig M., Evenson P., Humble J. and Pyle R. (2005) Addressing solar modulation and long-term uncertainties in scaling secondary cosmic rays for in situ cosmogenic nuclide applications. *Earth and Planetary Science Letters* **239**, 140-161.

Lifton N., Smart D. F. and Shea M. A. (2008) Scaling term time-integrated in situ cosmogenic nuclide production rates using a continuous geomagnetic model. *Earth and Planetary Science Letters* **268**, 190-201.

Masarik J. (2002) Numerical simulation of in-situ production of cosmogenic nuclides. *Goldschmidt Conference Abstract* **A491**.

Merchel S., Arnold M., Aumaître G., Benedetti L., Bourlès D. L., Braucher R., Alfimov V., Freeman S., Steier P. and Wallner A. (2008) Towards more precise ^{10}Be and ^{36}Cl data from measurements at the 10^{-14} level: Influence of sample preparation. *Nuclear Instruments and Methods in Physics Research Section B* **266**, 4921–4926.

Metropolis N., Rosenbluth A. W., Rosenbluth M. N. and Teller A. H. (1953) Equation of state calculations by fast computing machines. *Journal of Chemical Physics* **21**, 1087-1092.

Michel R., Lüpke M., Herpers U., Rösel R., Suter M., Dittrich-Hannen B., Kubik P. W., Filges D. and Cloth P. (1995) Simulation and modelling of the interaction of galactic protons with stony meteoroids. *Planetary and Space Science* **43**, 557-572.

Muzikar P. and Granger D. (2006) Combining cosmogenic, stratigraphic, and paleomagnetic information using a Bayesian approach: General results and an application to Sterkfontein. *Earth and Planetary Science Letters* **243**, 400-408.

Nishiizumi K., Winterer E. L., Kohl C. P., Klein J., Middleton R., Lal D. and Arnold, J. R. (1989) Cosmic ray production rates of ^{10}Be and ^{26}Al in quartz from glacially polished rocks. *Journal of Geophysical Research* **94**, 17907-17915.

Phillips F. M., Stone W. D. and Fabryka-Martin J. T. (2001) An improved approach to calculating low-energy cosmic-ray neutron fluxes near the land/atmosphere interface. *Chemical Geology* **175**, 689-701.

Phillips F. M., Zreda M. G. and Flinsch M. R. (1996) A reevaluation of cosmogenic ^{36}Cl production rates in terrestrial rocks. *Geophysical Research Letters* **23**, 949-952.

R Development Core Team (2008) R: A Language and Environment for Statistical Computing. R Foundation for Statistical Computing, Vienna, Austria, ISBN 3-900051-07-0.

Robert C. P. and Casella G. (1999) Monte Carlo Statistical Methods. *Springer Texts in*

Statistics. Springer-Verlag, New York.

Rust D. and Kershaw S. (2000) Holocene tectonic uplift patterns in northeastern Sicily: evidence from marine notches in coastal outcrops. *Marine Geology* **167**, 105-126.

Schildgen T., Phillips W. and Purves R. (2005) Simulation of snow shielding corrections for cosmogenic nuclide surface exposure studies. *Geomorphology* 64, 67-85.

Schimmelpfennig I. (2009) Cosmogenic ^{36}Cl in Ca and K rich minerals: analytical developments, production rate calibrations and cross calibration with ^{3}He and ^{21}Ne. PhD Thesis, Université Aix-Marseille III, France. (Also available at http://tel.archives-ouvertes.fr/tel-00468337/fr)

Schimmelpfennig I., Benedetti L., Finkel R., Pik R., Blard P. H., Bourlès D., Burnard P. and Williams A. (2009) Sources of in-situ ^{36}Cl in basaltic rocks. Implications for calibration of production rates. *Quaternary Geochronology* **4**, 441-461.

Schlagenhauf A., Gaudemer Y., Benedetti L., Manighetti I., Palumbo L., Schimmelpfennig I., Finkel R. and Pou K. (2010) Using in-situ chlorine-36 cosmonuclide to recover past earthquake histories on limestone normal fault scarps: A reappraisal of methodology and interpretations. *Geophysical Journal International* **182**, 36-72.

Sharma P., Kubik P. W., Fehn U., Gove H. E., Nishiizumi K. and Elmore D. (1990) Development of ^{36}Cl standards for AMS. *Nuclear Instruments and Methods in Physics Research Section B* **52**, 410-415.

Stone J. O. (2000) Air pressure and cosmogenic isotope production. *Journal of Geophysical Research* **105**, 23,753-23,759.

Stone J. O. (2005) Terrestrial chlorine-36 production from spallation of iron. *Abstract of 10th International Conference on Accelerator Mass Spectrometry.*

Stone J. O., Allan G. L., Fifield L. K. and Cresswell R. G. (1996) Cosmogenic ^{36}Cl from calcium spallation. *Geochimica et Cosmochimica Acta* **60**, 679-692.

Stone J. O., Evans J. M., Fifield L. K., Allan G. L. and Cresswell R. G. (1998) Cosmogenic ^{36}Cl production in calcite by muons. *Geochimica et Cosmochimica Acta* **62**, 433-454.

Stuiver M. and Reimer P. J. (1986) A computer program for radiocarbon age calibration. In *Proceedings of the 13th International ^{14}C Conference* (eds. M. Stuiver and R.S. Kra). *Radiocarbon* **28**, 1022-1030.

Swanson T. W. and Caffee M. L. (2001) Determination of ^{36}Cl production rates derived from the well-dated deglaciation surfaces of Whidbey and Fidalgo Islands, Washington. *Quaternary Research* **56**, 366-382.

Taylor J. R. (1997) An Introduction to Error Analysis. The Study of Uncertainties in Physical Measurements. *University Science Books*, Sausalito, USA.

Tanguy J.-C., Condomines M. and Kieffer G. (1997) Evolution of the Mount Etna magma: Constraints on the present feeding system and eruptive mechanism. *Journal of Volcanology and Geothermal Research* **75**, 221-250.

Zreda M. G., Phillips F. M., Elmore D., Kubik P. W., Sharma P. and Dorn R. I. (1991) Cosmogenic chlorine-36 production rates in terrestrial rocks. *Earth and Planetary Science Letters* **105**, 94-109.

Table captions:

Table 1: Previous published ^{36}Cl production rate studies and their calculation methods.

Table 2: Sample locations and description.

Table 3: Erosion rate calculations for sample SI41 determined from measured cosmogenic ^{3}He concentration in the same sample using five different scaling methods (attenuation length 177 g cm^{-2}, Farber et al., 2008; density 2.52 g cm^{-3}; the independent age 32.4 ± 1.3 ka).

Table 4: Results chemical analysis of minerals. ^{36}Cl and Cl concentrations are determined by AMS at LLNL-CAMS and the major element concentrations by ICP-OES at SARM-CRPG.

Table 5: Estimation of ^{36}Cl contributions from both major (Ca and K spallation) and minor reactions (low-energy neutron capture on Cl, muons, spallation of Ti, Fe) in the plagioclases from Mt. Etna and the sanidines from Payun Matru. Calculations were used as a guide to assess relative magnitudes using the ^{36}Cl spreadsheet in Schimmelpfennig et al. (2009) with the listed default values for the SLHL production rates and parameters. Production rates are scaled according to Stone (2000).

Table 6: Scaling methods used for the calibration, corresponding geomagnetic field models and database. Calculations, data input and database of each method follow as strictly as possible the respective study.

Table 7: Calibrated ^{36}Cl spallation production rates from Ca and K, normalised to SLHL with five published scaling schemes: St (Stone, 2000), Du (Dunai, 2001), De (Desilets et al., 2006a), Li05 (Lifton et al., 2005), Li08 (Lifton et al., 2008). a) All uncertainties are included in the calculations. b) Only the uncertainties in the independent age constraints are included. c) No uncertainty in the parameters of the data set is included. For the Historical Flow and the Solicchiata flow, the center between the minimum and maximum value of their uniform distributions were used as independent age value.

Table 8: ^{36}Cl exposure ages of the Etna and Payun Matru lava flows, resulting as output (posterior distributions) from the statistical algorithm according to the calibration results.

Table 9: ^{36}Cl exposure ages of the calibration samples, recalculated with the ^{36}Cl calculation spreadsheet (Schimmelpfennig et al., 2009) according to the calibration results. Uncertainties are derived by a standard error propagation, including uncertainties in the chemical analysis, the SLHL spallation production rates, all correction and scaling factors, 10% uncertainty in production from thermal and epithermal neutrons and 25% in the production from slow negative muons. Errors are missing for the exposure ages of the eroding flow La Nave, because the ages were determined by minimizing the difference between measured and calculated ^{36}Cl concentrations, taking into account the erosion rates.

Figure captions:

Fig. 1: Geographic locations of sample sites at Mt. Etna (38°N) and volcano Payun Matru (36°S).

Fig. 2: Pictures of sample surfaces at Mt. Etna.

Fig. 3: Pictures of sample surfaces at Payun Matru.

Fig. 4: Measured ^{36}Cl concentrations in the calibration samples, determined from AMS isotope dilution measurements, corrected for ^{36}Cl background contributions in spike and acids introduced during chemical processing.

Fig. 5: Feldspar ternary diagram with compositional signature of the calibration minerals. Etna plagioclases have labradorite composition, i.e. Ca is the dominant ^{36}Cl target element, while Payun Matru alkali-feldspars are sanidines, i.e. K is the dominant ^{36}Cl target element.

Fig. 6: Normalized scaling factors for spallation reactions (a) and slow negative muon capture (b) for each calibration site according to the five different scaling methods. Scaling factors derived from Du (Dunai 2001), De (Desilets et al., 2006a), Li05 (Lifton et al., 2005) and Li08 (Lifton et al., 2008) are normalized to those derived from St (Stone 2000) to display the differences between the methods in function of the altitude of the sample site and the exposure duration of the flows. Absolute values derived from St are displayed in (c) and those derived from all scaling methods are listed in Table A.2. In the case of the four methods that consider temporal variations (Du, De, Li05 and Li08), the scaling factors were integrated over the following time spans: Historical Flow 0-400 years, Solicchiata 0-8 ka, Piano della Lepre 10-20 ka, La Nave 0-32 ka, Payun Matru 0-15 ka.

Fig. 7: Posterior distributions of PR_{Ca} and PR_{K} resulting from the Bayesian statistical analysis of the calibration data set. Scaling according to Stone (2000).

Fig. 8: Recalculated ^{36}Cl ages for each lava flow compared to independent ages (see section 3.1). Exposure ages are shown for St (a) and Li08 (b) scaling as described in the text. Each panel shows the independent ages (squares with 1σ error bars or black closed intervals representing uniform distributions). Circles are ^{36}Cl exposure ages recalculated with the ^{36}Cl calculation spreadsheet (Schimmelpfennig et al., 2009). Diamonds are exposure ages resulting as model output from the statistical algorithm, also illustrated by the shaded zone.

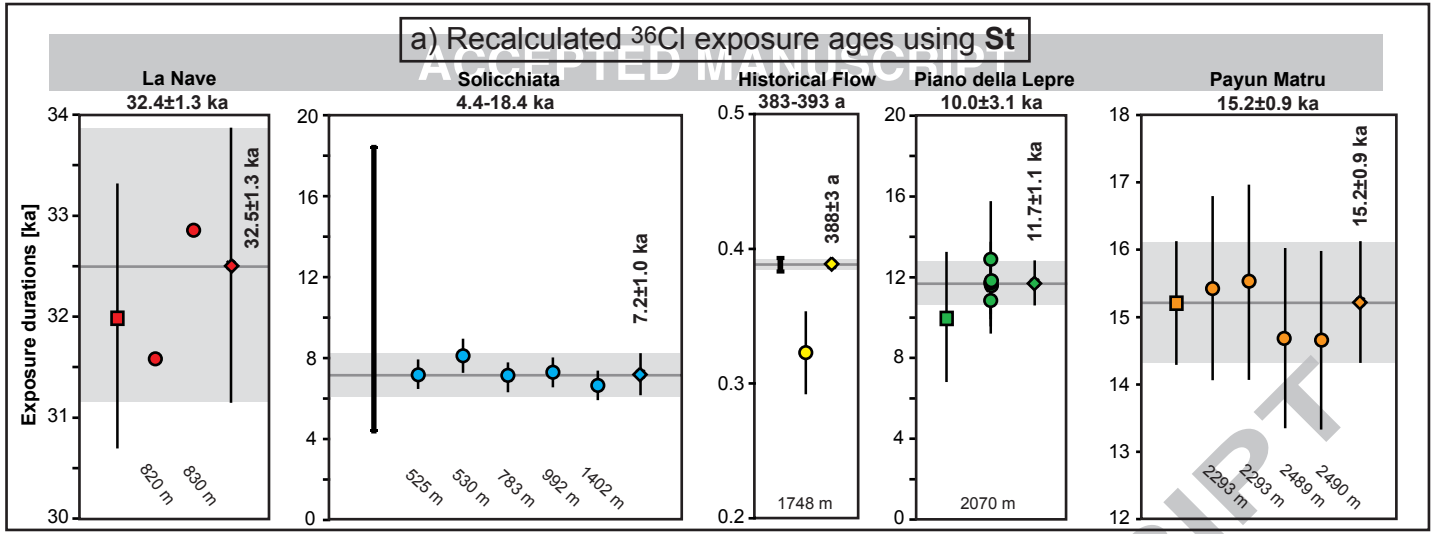

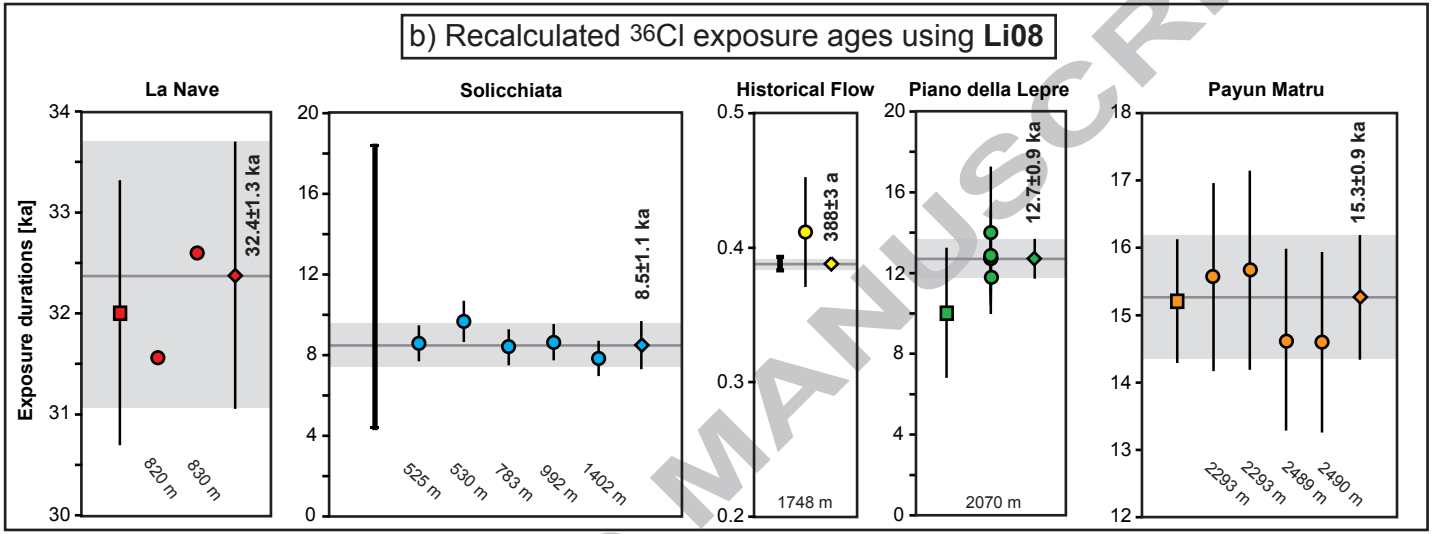

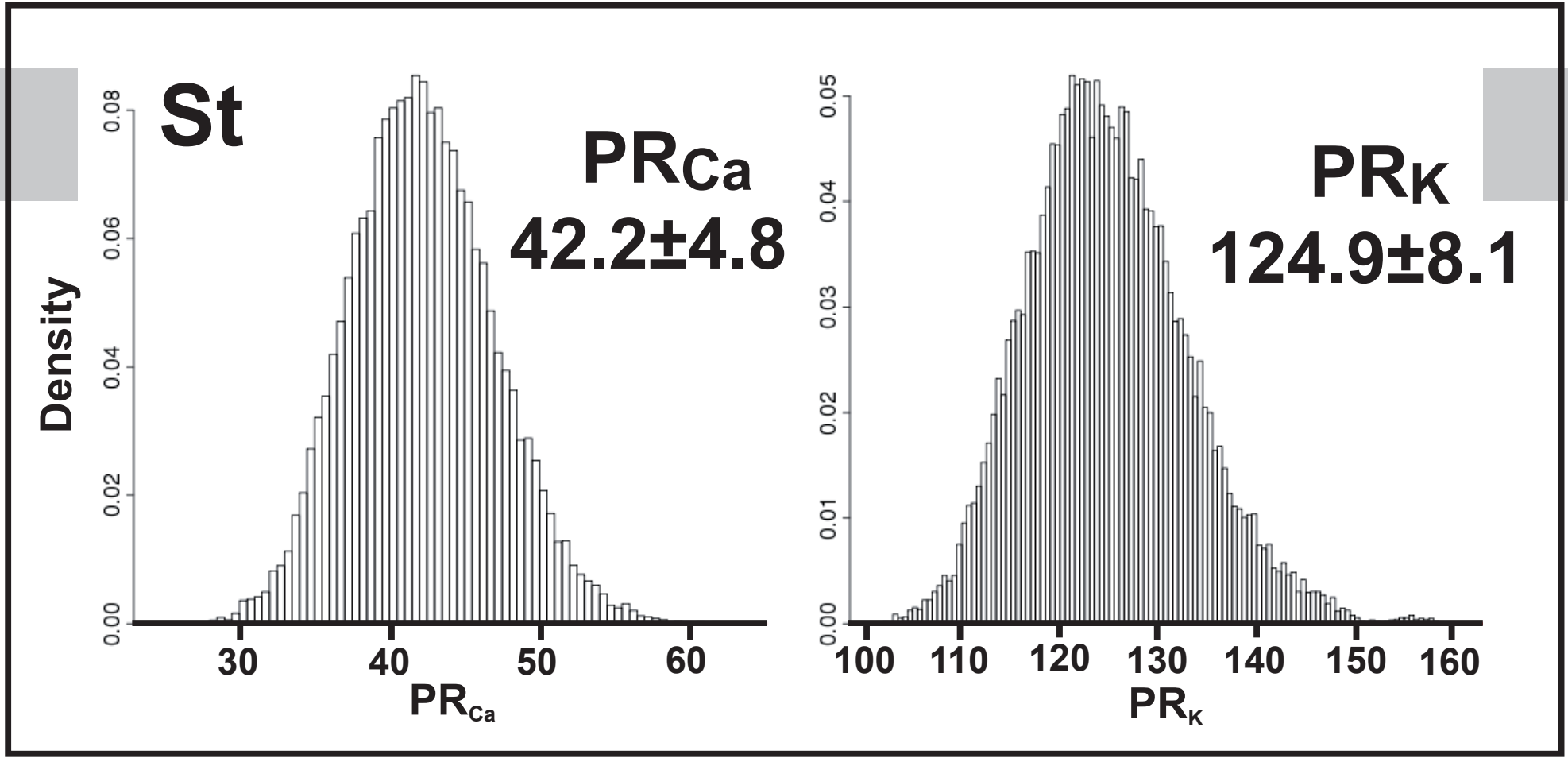
St
PRCa
42.2±4.8
PRK
124.9±8.1
Density
0.00
0.02
0.04
0.06
0.08
30
40
50
60
PRCa
0.00
0.01
0.02
0.03
0.04
0.05
100
110
120
130
140
150
160
PRK

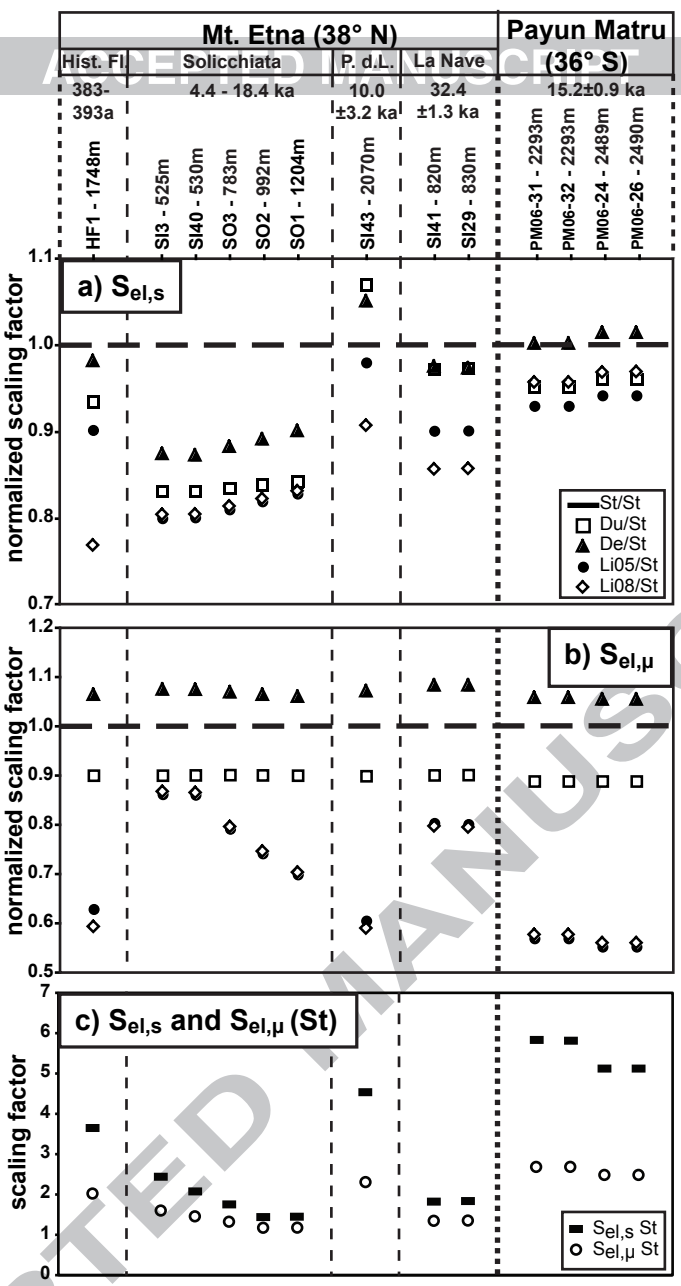

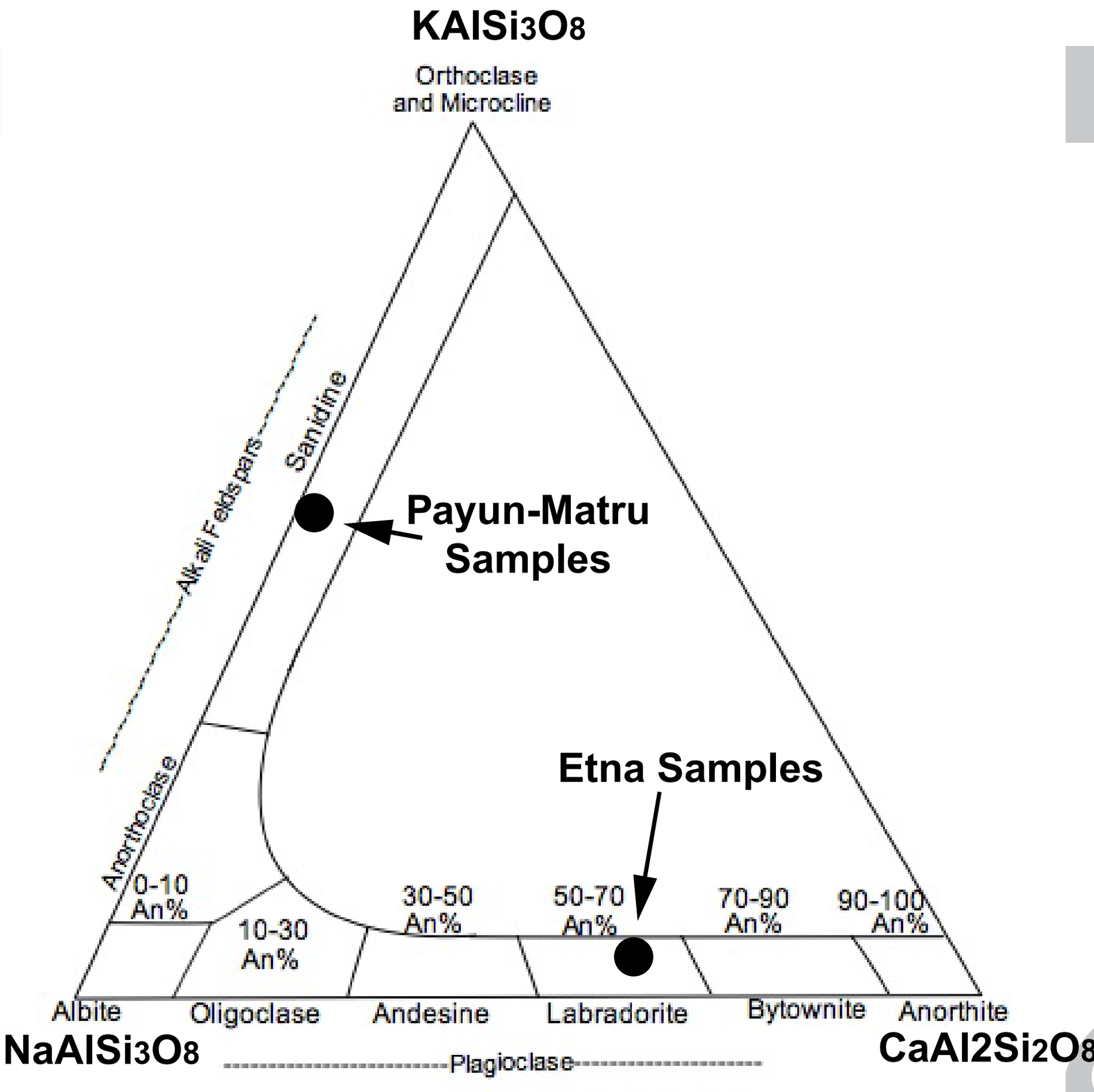
KAlSi3O8
Orthoclase
and Microcline
Alkali Feldspars
Sanidine
Payun-Matru
Samples
Etna Samples
Anorthoclase
0-10
An%
10-30
An%
30-50
An%
50-70
An%
70-90
An%
90-100
An%
Albite
Oligoclase
Andesine
Labradorite
Bytownite
Anorthite
NaAlSi3O8
Plagioclase
CaAl2Si2O8

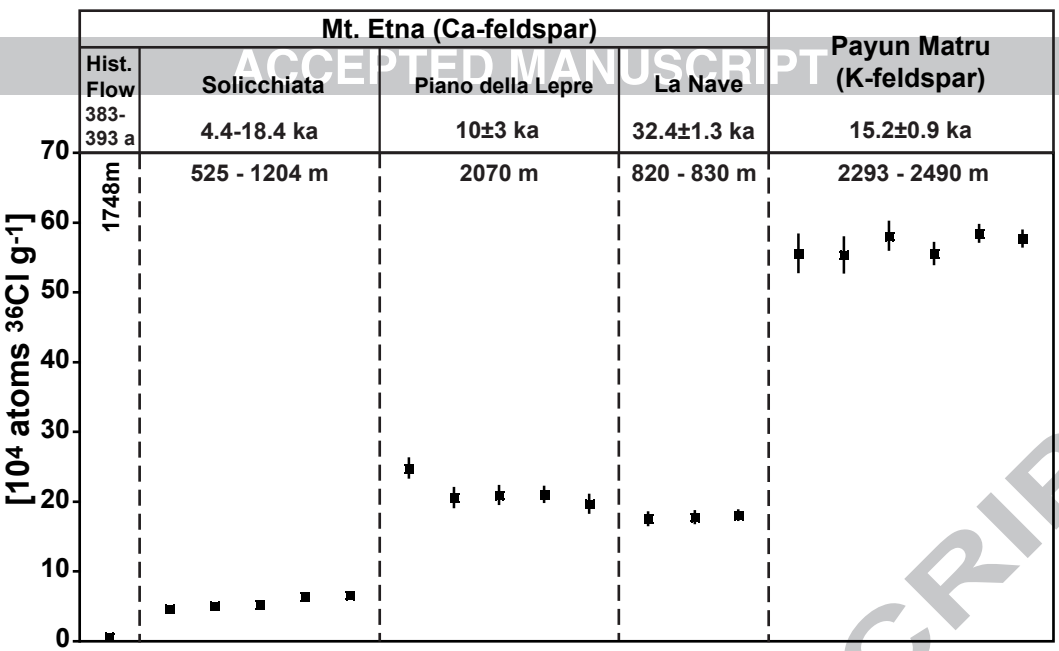


PM06-24


PM06-26


PM06-31
sampled bit


PM06-32

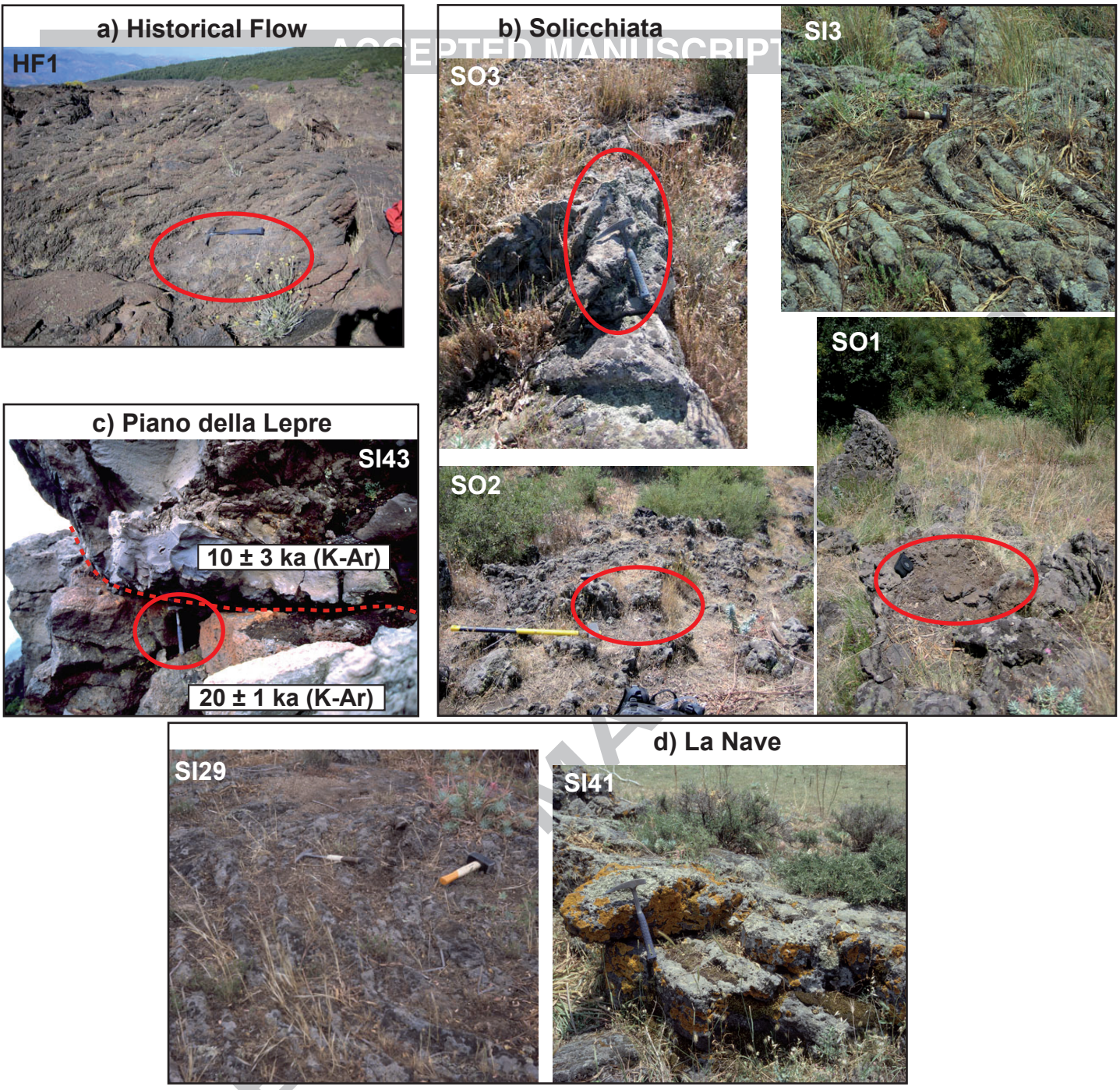

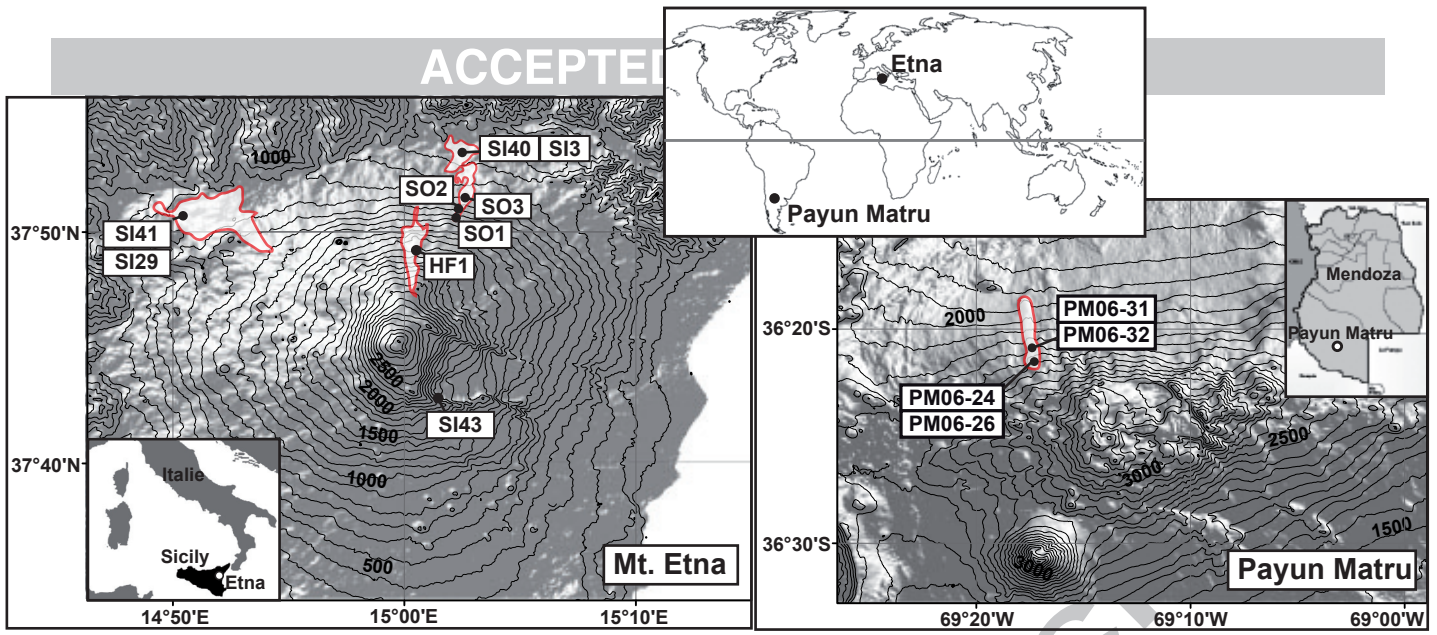
Etna
Payun Matru
SI40
SI3
SO2
SO3
SO1
HF1
SI41
SI29
SI43
1000
2500
2000
1500
1000
500
37°50'N
37°40'N
14°50'E
15°00'E
15°10'E
Italie
Sicily
Etna
Mt. Etna
PM06-31
PM06-32
PM06-24
PM06-26
2000
3000
2500
1500
3500
36°20'S
36°30'S
69°20'W
69°10'W
69°00'W
Mendoza
Payun Matru
Payun Matru

Table 1: *Previous published ^{36}Cl production rate studies and their calculation methods.*

Study	Calibrated SLHL production rates[a]	Sample number	Sample material (and Cl content)	Sample locations and independent ages	Scaling method	Calculation method
Zreda et al. (1991)	PR_{Ca} = 76±5* PR_K = 106±8* PR(^{35}Cl(n,γ)^{36}Cl) = 307±24	9	Basaltic whole rock, Microcline, Quartz (94-160 ppm Cl)	Latitude 37°-39°N Longitude 119°-113°W Elevation 1400-3800 m Exposure ages 9.7-14.4 ka	Lal (1991)	For each sample: best estimate of one of the 3 production rates, depending on prevailing target element, iteratively solved for the whole dataset. Global value for each PR by least square algorithm in function of the target element concentrations.
Phillips et al. (1996)	PR_{Ca} = 73±5* PR_K = 154±10* $P_f(0)$ = 586±40	33	Whole silicate rocks (6-350 ppm Cl)	Latitude 20°-80°N Longitude 3-160°W Elevation 20-2600 m Exposure ages 3-55 ka	Lal (1991); corrections for temporal variations according to Nishiizumi (1989)	Based on a small number of selected samples: minimizing the coefficient of variation of the ratios PR_K/PR_{Ca} and $P_f(0)/PR_{Ca}$. For the whole dataset: best estimate for PR_{Ca} by minimizing the reduced χ^2 parameter comparing calculated and independent ages.
Stone et al. (1996)	PR_{Ca} = 48.8±1.7	3	Ca-feldspar (2-5 ppm Cl)	Latitude 38.9°N Longitude 112°W Elevation 1445 m Exposure age 17.3 ka	Lal (1991); corrections for temporal variations similar to Nishiizumi (1989)	PR_{Ca} calculated by a standard χ^2 fitting procedure, minimizing the sum of inverse-error-weighted difference between calculated and measured ^{36}Cl concentrations. Uncertainties derived from a 400 point Monte-Carlo error propagation including full analytical uncertainties, ±20% in P_K, P(^{35}Cl(n,γ)^{36}Cl) and ±25% in P_μ.
Evans et al. (1997)	PR_K = 170±25*	11	K-feldspar (9-315 ppm Cl)[c]	Latitudes 38° N, 58°N Longitude 120°W, 4°W Elevation 3000-3600 m, 520 m Exposure ages 13.1 ka, 11.6 ka	Lal (1991)	Not specified
Phillips et al. (2001)	PR_{Ca} = 66.8±4.4 PR_K = 137±9 $P_f(0)$ = 626±46	30	Same as Phillips et al. (1996)	Latitude 35°-80°N Longitude 3-160°W Elevation 20-2600 m Exposure ages 3-49 ka	Same as Phillips et al. (1996)	Same as Phillips et al. (1996)
Swanson and Caffee (2001)	PR_{Ca} = 91±5* PR_K = 228±18* $P_f(0)$ = 762±28	37[b]	Whole silicate rocks (42-290 ppm Cl)	Latitude 48°N Longitude 122°W Elevation 10-140 m Exposure age 15.5 ka	Lal (1991)	For each sample: best estimate of either $P_f(0)$, PR_{Ca} or PR_K, depending on the prevailing target element. Mean value for each production rate.
Licciardi et al. (2008)	PR_{Ca} = 52±5[d]	21	Whole basaltic rock (29-61 ppm Cl)	Latitude 64°N Longitude 21-22°W Elevation 20-460 m Exposure ages 4-10 ka	Lal (1991), Stone (2000)	For each sample: PR_{Ca} is iteratively adjusted until the calculated age matches the independent age. Mean value of each of the four lava flows. Grand mean of the four flows with standard deviation of the grand mean as error.

* Values are not corrected for ^{36}Cl production from slow negative muon capture, the others are production rates only from spallation.

[a] Units for PR_{Ca} and PR_K: [atoms ^{36}Cl (g target element)$^{-1}$ a^{-1}] Unit for $P_f(0)$, the production rate of epithermal neutrons from the fast neutron flux in the atmosphere: [neutrons (g air)$^{-1}$ a^{-1}]. Unit for PR(^{35}Cl(n,γ)^{36}Cl): [neutrons (g rock)$^{-1}$ a^{-1}].

[b] Swanson and Caffee (2001): It is not clear if the dataset contains replicates.

[c] Evans et al. (1997): Cl and associated ^{36}Cl was partly released from fluid inclusions by crushing mineral aliquots in order to quantify the ^{36}Cl contribution due to ^{35}Cl(n,γ)^{36}Cl.

[d] PR_{Ca} in Licciardi et al. (2008) is corrected for abnormal pressure effects at the Icelandic calibration site. Assuming normal pressure conditions results in 57 ± 5 atoms ^{36}Cl (g target element)$^{-1}$ a^{-1}.

Table 2: *Sample locations and description.*

Sample	Altitude [m]	latitude	longitude	Lava morphology	Thickness [cm]	density [g cm^{-3}][a]
Mt. Etna: Historic Flow 1614-24 (between 383 and 393 years)						
HF1	1748	N 37.82°	E 15.01°	Pahoehoe cords	4	2.50
Mt. Etna: Solicchiata (^{14}C between 4.4 ka and 18.4 ka)						
SI3	525	N 37.89°	E 15.09°	Pahoehoe cords	5	2.57
SI40	530	N 37.90°	E 15.07°	Pahoehoe cords	10	2.57
SO3	783	N 37.86°	E 15.07°	Pahoehoe cords	9.5	2.38
SO2	992	N 37.84°	E 15.07°	Pahoehoe cords	8	2.45
SO1	1204	N 37.84°	E 15.06°	Pahoehoe cords	12	2.30
Mt. Etna: Piano della Lepre (K-Ar 10.0 ± 3.2 ka)						
SI43	2070	N 37.71°	E 15.03°	Pahoehoe, fossil-exposed	15	2.37
Mt. Etna: La Nave (K-Ar/TL 32.4 ± 1.3 ka)						
SI41	820	N 37.85°	E 14.84°	Pahoehoe cords, eroded	15	2.52
SI29	830	N 37.85°	E 14.83°	Pahoehoe cords, eroded	10	2.52
Payun Matru (K-Ar 15.2 ± 0.9 ka)						
PM06-31	2293	S 36.35°	W 69.29°	aa-block	4	2.30
PM06-32	2293	S 36.35°	W 69.29°	aa-block	4	2.30
PM06-24	2489	S 36.36°	W 69.29°	aa-block	4	2.30
PM06-26	2490	S 36.36°	W 69.29°	aa-block	4	2.30

[a] Densities were determined using the Archimedes principle.

Table 3: *Erosion rate calculations for sample SI41 determined from measured cosmogenic ^{3}He concentration in the same sample using five different scaling methods (attenuation length 177 g cm^{-2}, Farber et al., 2008; density 2.52 g cm^{-3}; the independent age 32.4 ± 1.3 ka).*

Scaling method	Spallation scaling factor	Erosion rate [mm/ka]
St	1.823	11.1 ± 3.3
Du	1.773	9.8 ± 2.9
De	1.776	9.9 ± 3.0
Li05	1.642	6.4 ± 1.0
Li08	1.561	4.1 ± 1.2

Table 4: *Results chemical analysis of minerals.* ^{36}Cl *and Cl concentrations are determined by AMS at LLNL-CAMS and the major element concentrations by ICP-OES at SARM-CRPG.*

Sample	Grain size [μm]	Sample weight dissolved [g]	$^{35}Cl/^{37}Cl$	^{36}Cl/(stable Cl)[a] [10^{-14}]	Amount carrier [mg Cl][b]	Cl [ppm]	^{36}Cl [10^4 at/g]	Blank correction	Ca [wt%]	K [wt%]	Ti [wt%]	Fe [wt%]
Mt. Etna: Historic Flow 1614-24 (between 383 and 393 years)												
HF1[c]	100-400	341.76	0.5272± 0.0015	6.89± 0.18	1.521	3.5± 0.2	0.50±0.02	15%	8.2± 0.2	0.36± 0.05	0.05± 0.01	0.48± 0.02
Mt. Etna: Solicchiata (^{14}C between 4.4 ka and 18.4 ka)												
SI3[c]	100-400	35.83	0.1199± 0.0014	7.66± 0.22	1.519	5.6± 0.3	4.52± 0.18	16%	8.4± 0.2	0.30± 0.04	0.05± 0.01	0.52± 0.03
SI40[c]	100-400	40.20	0.1191± 0.0014	9.18± 0.33	1.519	5.0± 0.3	4.98± 0.22	13%	8.3± 0.2	0.29± 0.04	0.05± 0.01	0.51± 0.03
SO3[c]	100-400	37.17	0.0922± 0.0044	8.94± 0.30	1.518	3.9± 0.3	5.16± 0.22	14%	8.2± 0.2	0.29± 0.04	0.05± 0.01	0.50± 0.03
SO2[c]	100-400	32.79	0.0654± 0.0008	9.66± 0.25	1.521	2.7± 0.2	6.34± 0.21	13%	8.4± 0.2	0.29± 0.04	0.05± 0.01	0.50± 0.03
SO1[c]	100-400	21.41	0.0541± 0.0005	6.91± 0.26	1.522	3.1± 0.2	6.50± 0.33	18%	8.2± 0.2	0.29± 0.04	0.05± 0.01	0.50± 0.03
Mt. Etna: Piano della Lepre (K-Ar 10.0 ± 3.2 ka)												
SI43-D4*[f]	140-400	5.03	80.13± 0.51	5.18± 0.16	1.796	2.8± 1.0	23.3± 1.4[g]	25%	8.9± 1.9	0.58± 0.31	0.07± 0.08	0.59± 0.32
SI43-D5*[f]	140-400	4.97	78.91± 0.41	4.48± 0.16	1.792	3.1± 1.0	19.4± 1.4[g]	29%	6.6± 1.7	0.44± 0.27	0.06± 0.07	0.46± 0.28
SI43-D6*[f]	140-400	7.50	56.13± 0.57	6.36± 0.23	1.794	2.5± 1.0	19.6± 1.3[g]	24%	7.5± 0.6	0.46± 0.09	0.06± 0.02	0.50± 0.10
SI43-D7*[f]	140-400	9.77	46.01± 0.59	7.94± 0.21	1.800	2.0± 1.0	19.7± 1.1[g]	22%	7.4± 0.4	0.48± 0.07	0.06± 0.02	0.48± 0.07
SI43-D8*[f]	140-400	13.06	32.32± 0.36	9.83± 0.33	1.792	1.2± 1.0	18.4± 1.3[g]	23%	7.6± 0.2	0.48± 0.02	0.06± 0.01	0.50± 0.03
Mt. Etna: La Nave (K-Ar/TL 32.4 ± 1.3 ka)												
SI41[c]	140-400	8.98	0.0367± 0.0052	7.67± 0.30	1.519	3.4± 1.2	17.44± 0.88	17%	7.4± 0.2	0.45± 0.03	0.06± 0.01	0.45± 0.02
SI29-160[c]	100-160	8.06	0.0327± 0.0004	7.11± 0.24	1.518	2.8± 0.2	17.69± 0.83	18%	7.1± 0.1	0.42± 0.03	0.06± 0.01	0.41± 0.02
SI29-250[c]	160-250	9.91	0.0327± 0.0004	8.54± 0.24	1.522	2.3± 0.2	17.96± 0.67	15%	7.2± 0.1	0.43± 0.03	0.06± 0.01	0.42± 0.02
Payun Matru (K-Ar 15.2 ± 0.9 ka)												
PM06-31[c]	250-1400	5.50	0.0428± 0.0001	13.78± 0.58	1.510	7.7± 0.5	55.5± 2.7	9%	0.54± 0.03	5.4± 0.1	0.03± 0.01	0.19± 0.01
PM06-31-Rep[c]	250-1400	5.28	0.0428± 0.0001	13.18± 0.52	1.516	8.1± 0.5	55.3± 2.5	10%	0.54± 0.03	5.4± 0.1	0.03± 0.01	0.19± 0.01
PM06-32[c]	250-1400	9.59	0.0856± 0.0003	23.56± 0.75	1.521	13.6± 0.7	58.0± 2.0	5%	0.55± 0.03	5.4± 0.1	0.03± 0.01	0.19± 0.01
PM06-32-Rep[c]	250-1400	8.35	0.0749± 0.0002	19.95± 0.48	1.518	12.9± 0.7	55.5± 1.5	6%	0.55± 0.03	5.4± 0.1	0.03± 0.01	0.19± 0.01
PM06-24*[d]	250-1400	7.37	104.49± 0.91	17.46± 0.24	1.470	6.4± 0.4	58.4± 1.2	5%	0.55± 0.03	5.3± 0.1	0.03± 0.01	0.18± 0.01
PM06-26*[e]	250-1400	7.61	74.95± 0.40	17.66± 0.31	1.466	9.2± 0.5	57.6± 1.1	5%	0.52± 0.03	5.2± 0.1	0.03± 0.01	0.19± 0.01
		acid mixture [ml]				Cl [10^{16} atoms]	^{36}Cl [10^5 atoms]					
Blank Bl1		30	0.0214± 0.0001	1.28± 0.10	1.517	10.27±0.5	3.11±0.32					
Blank BLH-D1*		15	171.91± 0.31	1.032± 0.058	1.802	62.8±3.3	3.25±0.18					
Blank BLH-D2*		24	122.98± 0.17	1.32± 0.24	1.802	93.6±4.6	4.17±0.75					
Blank BLH-D3*		30	100.44± 0.45	1.220± 0.073	1.802	118.3±5.9	3.89±0.23					
Blank Bl2*		100	432.0± 4.9	0.969± 0.065	1.465	13.76±0.73	2.45±0.17					
Blank Bl3*		100	482.04± 8.80	0.933± 0.064	1.475	11.31±0.69	2.38±0.16					

[a] The measured $^{36}Cl/(\text{stable Cl})$ ratio is $^{36}Cl/^{37}Cl$ for most of the samples and $^{36}Cl/^{35}Cl$ for those accompanied by an asterisk.

[b],* The Cl carrier is enriched in ^{35}Cl (99.90 atomic %) for those accompanied by an asterisk and enriched in ^{37}Cl (98.21 atomic %) for the others.

[c] Samples corrected with blank Bl1 in terms of number of atoms ^{36}Cl and Cl.

[d] Sample corrected with blank Bl3 in terms of number of atoms ^{36}Cl and Cl.

[e] Sample corrected with blank Bl2 in terms of number of atoms ^{36}Cl and Cl.

[f] Samples corrected with blanks BLH-D1, BLH-D2, BLH-D3 in terms of number of atoms ^{36}Cl and Cl and according to the amount of acid used.

[g] The measured ^{36}Cl concentrations of SI43 were corrected for the calculated non-fossil component, which is the ^{36}Cl production in 250 cm depth since the surface was covered by an superposed flow (for details see Schimmelpfennig et al., 2009). The calculated non-fossil component accounts for about 6% of the total ^{36}Cl inventory.

Table 5: *Estimation of ^{36}Cl contributions from both major (Ca and K spallation) and minor reactions (low-energy neutron capture on Cl, muons, spallation of Ti, Fe) in the plagioclases from Mt. Etna and the sanidines from Payun Matru. Calculations were used as a guide to assess relative magnitudes using the ^{36}Cl spreadsheet in Schimmelpfennig et al. (2009) with the listed default values for the SLHL production rates and parameters. Production rates are scaled according to Stone (2000).*

Production mechanism	Default values for ^{36}Cl prod. rates and parameters at SLHL	^{36}Cl Contribution in plagioclases from Mt. Etna	^{36}Cl Contribution in sanidines from Payun Matru
Spallation on Ca, K, Ti and Fe		86.6 - 92.7%	94.8 - 96.7%
Spallation on Ca	48.8±1.7 at (g Ca)$^{-1}$a^{-1} (Stone et al., 1996)	74.3 - 79.9%	2.8 - 2.9%
Spallation on K	162±25 at (g K)$^{-1}$a^{-1} (Evans et al., 1997)	8.9 - 16.4%	91.9 - 93.7%
Spallation on Ti	13±3 at (g Ti)$^{-1}$a^{-1} (Fink et al., 2000)	0.1 - 0.2%	0.04%
Spallation on Fe	1.9 at (g Fe)$^{-1}$a^{-1} (Stone, 2005)	0.2%	0.04%
Low-energy neutron capture by ^{35}Cl	626 neutrons (g air)$^{-1}$a^{-1} (Phillips et al., 2001)	0.9 - 3.1%	1.7 - 3.5%
Slow-negative muon capture by Ca and K	190 μ g^{-1}a^{-1} (Heisinger et al., 2002)	6.3 - 10.2%	1.6 - 1.7%

[a] After Evans et al. (1997) the total production rate from K, including spallation and slow negative muon capture, is 170 ± 25 atoms ^{36}Cl (g K)$^{-1}$a^{-1} with a contribution from muons of about 5%, which results in a spallation production rate of 162 atoms ^{36}Cl (g K)$^{-1}$a^{-1}.

Table 6: *Scaling methods used for the calibration, corresponding geomagnetic field models and database. Calculations, data input and database of each method follow as strictly as possible the respective study.*

Scaling scheme[a]	Geomagnetic field model	Method of calculating R_c	Input for the latitude effect	Input for the elevation effect	Calculation of slow negative muon scaling factor	Comments
St	/	/	Geographic latitude	Atmospheric pressure	Eq. 3 in Stone 2000	- not taking into account temporal variations
Du	<10 ka: non-dipole field with local record of paleoinclination from Brandt et al. (1999) (42.5°N, near Mt. Etna calibration site) >10 ka: GAD[b]	<10 ka: Eq. 2 in Du (dipolar approximation taking into account local paleoinclination and horizontal field strength) - M_c from Ohno and Hamano (1993) >10 ka: Eq.1 in Du - Mc from Yang et al. (2000) (0-11 ka) and SINT800[d] (11-150 ka)	<10 ka: geomagnetic latitude from geographic latitude and longitude[f] and paleopoleposition of northpole from Ohno and Hamano (1993) >10 ka: geographic latitude	Atmospheric depth (g cm-2)	Eq. 8 in Dunai 2000 with Λ_μ = 247 g cm-2 (not taking into account temporal variations)	
De	GAD[b]	Eq. 19 in Desilets and Zreda (2003) (best-fit model based on R_c from trajectory tracing assuming a GAD[b]) - M/M_0 with M_0 from 1950 DGRF[e] - M[c] from Yang et al. (2000) (0-11 ka) and SINT800[d] (11-150 ka)	<10 ka: dipolar geomagnetic latitude from geographic latitude and longitude[g] and paleopoleposition of northpole from Merrill and McElhinny (1983) (0-2 ka) and Ohno and Hamano (1993) (2-10 ka) >10 ka: geographic latitude	Atmospheric depth (g cm-2)	Latitude effect: Eq. 3 in Desilets and Zreda (2003) with α = 38.51 and k =1.03 Elevation effect: Eq. 2 in Desilets and Zreda (2003) with Λ_μ according to Eq. 7 (taking into account temporal variations)	
Li05	GAD[b]	Eq. 6 in Li05 (best-fit model based on R_c from trajectory tracing, averaging current eccentric dipole and non-dipole fields) - M/M_0 with M_0 from 1950 DGRF[e] - M[c] from Yang et al. (2000) (0-11 ka) and SINT800[d] (11-150 ka)	<10 ka: dipolar geomagnetic latitude from geographic latitude and longitude[g] and paleopoleposition of northpole from Merrill and McElhinny (1983) (0-2 ka) and Ohno and Hamano (1993) (2-10 ka) >10 ka: geographic latitude	Atmospheric depth (g cm-2) - standard atmosphere	Eq. 2 in Li05 (taking into account temporal variations)	- Taking into account solar modulation - published spreadsheet in Appendix of Li05 used to integrate the spallation and muon scaling factors over the respective exposure durations
Li08	<7 ka: continuous non-dipole geomagnetic field model (CALS7K.2 from Korte and Constable, 2005) >7 ka: non-dipole field	0-7 ka: R_c from trajectory tracing based on spherical harmonic field model of Korte and Constable (2005) >7 ka: Eq. 4 in Li08 (best-fit model based on the mean CALS7K.2 field over the 0-7 ka period) - M/M_0 with M_0 from 1950 DGRF[e] - M[c] from SINT800[d]	<7 ka: geomagnetic latitude from geographic latitude and longitude[g] and paleopoleposition of northpole from Jackson et al. (2000) (0-0.3 ka) and Korte and Constable (2005) (0.3-7 ka) >7 ka: geographic latitude	Atmospheric depth (g cm-2) variable atmosphere	Eq. 2 in Li05 (taking into account temporal variations)	- Taking into account solar modulation - extended spreadsheet of Li05 used to find the spallation and muon scaling factors - predicts longitudinal variability

[a] St: Stone (2000), Du: Dunai (2001), De: Desilets et al. (2006), Li05: Lifton et al. (2005), Li08: Lifton et al. (2008).
[b] GAD: geocentric axial dipole field.
[c] M: dipole moment [Am^2].
[d] Guyodo and Valet (1999).
[e] Definitive Geomagnetic Reference Field.
[f] Positive values for latitude and longitude of Argentinean samples.
[g] Negative values for latitude and longitude of Argentinean samples.

ACCEPTED MANUSCRIPT

Table 7: *Calibrated ^{36}Cl spallation production rates from Ca and K, normalised to SLHL with five published scaling schemes: St (Stone, 2000), Du (Dunai, 2001), De (Desilets et al., 2006), Li05 (Lifton et al., 2005), Li08 (Lifton et al., 2008). a) All uncertainties are included in the calculations. b) Only the uncertainties in the independent age constraints are included. c) No uncertainty in the parameters of the data set is included. For the Historical Flow and Solicchiata flow, the center between the minimum and maximum value of their uniform distributions were used as independent age value.*

	Scaling method	SLHL PR_{Ca} [atoms ^{36}Cl (g Ca)$^{-1}$ a^{-1}] Mean $\pm\sigma$	SLHL PR_K [atoms ^{36}Cl (g K)$^{-1}$ a^{-1}] Mean $\pm\sigma$
a)	St	42.2 ± 4.8	124.9 ± 8.1
	Du	42.4 ± 4.7	130.9 ± 8.5
	De	41.6 ± 4.8	124.0 ± 8.4
	Li05	43.3 ± 3.8	135.1 ± 8.7
	Li08	44.0 ± 3.8	131.0 ± 8.5
b)	St	42.2 ± 3.0	124.5 ± 7.9
	Du	42.4 ± 3.2	131.4 ± 8.3
	De	41.6 ± 3.3	124.0 ± 8.7
	Li05	43.4 ± 3.4	135.2 ± 8.7
	Li08	44.0 ± 3.4	130.8 ± 8.6
c)	St	44.0 ± 2.8	124.4 ± 2.6
	Du	43.9 ± 2.0	131.0 ± 2.0
	De	43.5 ± 2.3	123.4 ± 2.1
	Li05	47.5 ± 2.4	134.8 ± 2.4
	Li08	50.0 ± 3.0	130.4 ± 2.7

Table 8: *^{36}Cl exposure ages of the Etna and Payun Matru lava flows, resulting as output (posterior distributions) from the statistical algorithm according to the calibration results.*

St	Du	De	Li05	Li08
Mt. Etna: Historic Flow 1614-24 (between 383 and 393 years)				
388 ± 3 a	388 ± 3 a	388 ± 3 a	388 ± 3 a	388 ± 3 a
Mt. Etna: Solicchiata (^{14}C between 4.4 ka and 18.4 ka)				
7.17 ± 0.97 ka	8.5 ± 1.2 ka	8.0 ± 1.2 ka	8.6 ± 1.2 ka	8.5 ± 1.1 ka
Mt. Etna: Piano della Lepre (K-Ar 10.0 ± 3.2 ka)				
11.7 ± 1.1 ka	10.9 ± 1.0 ka	11.3 ± 1.1 ka	11.86 ± 0.89 ka	12.68 ± 9.3 ka
Mt. Etna: La Nave (K-Ar/TL 32.4 ± 1.3 ka)				
32.4 ± 1.3 ka	32.5 ± 1.3 ka	32.4 ± 1.3 ka	32.4 ± 1.3 ka	32.4 ± 1.3 ka
Payun Matru (K-Ar 15.2 ± 0.9 ka)				
15.21 ± 0.89 ka	15.28 ± 0.90 ka	15.20 ± 0.92 ka	15.25 ± 0.89 ka	15.26 ± 0.91 ka

Table 9: *^{36}Cl exposure ages of the calibration samples, recalculated with the ^{36}Cl calculation spreadsheet (Schimmelpfennig et al., 2009) according to the calibration results. Uncertainties are derived by a standard error propagation, including uncertainties in the chemical analysis, the SLHL spallation production rates, all correction and scaling factors, 10% uncertainty in production from thermal and epithermal neutrons and 25% in the production from slow negative muons. Errors are missing for the exposure ages of the eroding flow La Nave, because the ages were determined by minimizing the difference between measured and calculated ^{36}Cl concentrations, taking into account the erosion rates.*

	St	Du	De	Li05	Li08
Mt. Etna: Historic Flow 1614-24 (between 383 and 393 years)					
HF1	322 ± 30 a	343 ± 33 a	330 ± 32 a	355 ± 35 a	411 ± 40 a
Mt. Etna: Solicchiata (^{14}C between 4.4 ka and 18.4 ka)					
SI3	7.17 ± 0.67 ka	8.50 ± 0.82 ka	8.10 ± 0.79 ka	8.66 ± 0.85 ka	8.55 ± 0.83 ka
SI40	8.09 ± 0.78 ka	9.59 ± 0.95 ka	9.13 ± 0.92 ka	9.77 ± 0.98 ka	9.64 ± 0.96 ka
SO3	7.02 ± 0.67 ka	8.29 ± 0.81 ka	7.87 ± 0.79 ka	8.46 ± 0.84 ka	8.36 ± 0.83 ka
SO2	7.26 ± 0.68 ka	8.55 ± 0.82 ka	8.09 ± 0.78 ka	8.72 ± 0.85 ka	8.61 ± 0.83 ka
SO1	6.62 ± 0.67 ka	7.76 ± 0.80 ka	7.31 ± 0.76 ka	7.90 ± 0.83 ka	7.80 ± 0.81 ka
Mt. Etna: Piano della Lepre (K-Ar 10.0 ± 3.2 ka)					
SI43-D4	11.5 ± 2.2 ka	10.7 ± 2.1 ka	11.0 ± 2.1 ka	11.7 ± 2.3 ka	12.5 ± 2.5 ka
SI43-D5	12.8 ± 2.9 ka	12.0 ± 2.7 ka	12.3 ± 2.8 ka	13.0 ± 3.0 ka	14.0 ± 3.2 ka
SI43-D6	11.6 ± 1.4 ka	10.9 ± 1.4 ka	11.2 ± 1.4 ka	11.8 ± 1.5 ka	12.7 ± 1.6 ka
SI43-D7	11.8 ± 1.3 ka	11.0 ± 1.2 ka	11.3 ± 1.3 ka	12.0 ± 1.4 ka	12.9 ± 1.5 ka
SI43-D8	10.8 ± 1.2 ka	10.1 ± 1.1 ka	10.4 ± 1.2 ka	11.0 ± 1.2 ka	11.8 ± 1.3 ka
Mt. Etna: La Nave (K-Ar/TL 32.4 ± 1.3 ka)					
SI41	31.6 ka	31.8 ka	31.7 ka	31.7 ka	31.6 ka
SI29-160	32.5 ka	32.7 ka	32.6 ka	32.5 ka	32.3 ka
SI29-250	33.2 ka	33.3 ka	33.3 ka	33.1 ka	32.9 ka
Payun Matru (K-Ar 15.2 ± 0.9 ka)					
PM06-31	15.5 ± 1.5 ka	15.5 ± 1.5 ka	15.5 ± 1.6 ka	15.6 ± 1.6 ka	15.6 ± 1.6 ka
PM06-31-Rep	15.4 ± 1.5 ka	15.4 ± 1.5 ka	15.4 ± 1.6 ka	15.5 ± 1.5 ka	15.5 ± 1.5 ka
PM06-32	15.8 ± 1.5 ka	15.9 ± 1.5 ka	15.9 ± 1.5 ka	16.0 ± 1.5 ka	16.0 ± 1.5 ka
PM06-32-Rep	15.2 ± 1.4 ka	15.2 ± 1.4 ka	15.2 ± 1.4 ka	15.3 ± 1.4 ka	15.3 ± 1.4 ka
PM06-24	14.7 ± 1.3 ka	14.6 ± 1.3 ka	14.6 ± 1.4 ka	14.6 ± 1.3 ka	14.6 ± 1.3 ka
PM06-26	14.6 ± 1.3 ka	14.6 ± 1.3 ka	14.5 ± 1.3 ka	14.6 ± 1.3 ka	14.6 ± 1.3 ka